Analysis of the laser-stimulated reaction: $NO_2^*+CO \rightarrow NO+CO_2$

Cite as: J. Chem. Phys. **68**, 1070 (1978); https://doi.org/10.1063/1.435798
Published Online: 11 August 2008

I. P. Herman, R. P. Mariella and A. Javan

Analysis of the laser-stimulated reaction[a]: $NO_2^* + CO \rightarrow NO + CO_2$

I. P. Herman,[b] R. P. Mariella, Jr.,[c] and A. Javan

Department of Physics, Massachusetts Institute of Technology, Cambridge, Massachusetts 02139
(Received 22 August 1977)

This paper describes the room temperature, gas phase reaction of NO_2, excited by various cw visible lasers, with CO to form NO and CO_2. The distilled CO_2 product is detected by laser-induced fluorescence. Using this technique, and previously measured relaxation rates, the determined reaction rate constant with 4880 Å excitation is $k_R = 3.2 \pm 1.2 \times 10^{-15}$ cc/molecule sec. The observed dependences on laser intensity and reactant concentration are in agreement with a proposed mechanism in which $NO_2^* + CO \rightarrow NO + CO_2$ is the main step. Other possible mechanisms are found to disagree with experimental evidence. k_R is found to increase smoothly by a factor of 10 as the exciting wavelength is decreased from 6125 to 4579 Å. This behavior is compared to a model in which RRK theory predicts reactivity and a step-ladder model describes relaxation. Using this RRK model fit, the observed activation energy is 1.8 ± 0.2 eV, which appears to be 0.3–0.7 eV higher than the thermal energy barrier.

I. INTRODUCTION

In recent years there has been intensive investigation in stimulating unimolecular and bimolecular chemical reactions via electronic and vibrational excitation of the reactants.[1] The interest in such studies stems both from the fundamental scientific need to fully understand and predict elementary chemical reactions and from practical needs, such as inexpensive isotope separation and chemical syntheses. This paper details the results of one such investigation.

The reaction of visible laser electronically excited NO_2 with CO, to form NO and CO_2, was first reported by the authors in an earlier communication.[2] This gas phase, room temperature reaction was observed to proceed at a rate far exceeding that of the associated thermal reaction. The extent of reaction was determined by laser-induced fluorescence of the distilled CO_2 produced by laser irradiation with a CO_2 laser. In this paper further experimental details and results are presented, including a discussion of the fluorescence detection scheme and a model of the reaction dynamics.

In Sec. II the motives for undertaking this study are presented. This includes a discussion of the associated thermal reaction, the correlation of reactants to products, and the proposed reaction mechanism. The components of the experimental apparatus and the experimental technique are then described in Sec. III, followed by a detailed discussion of the method of CO_2 product detection in Sec. IV. The outcome of the experimental studies of the reaction's dependence on laser intensity and wavelength and on reactant concentration are presented in Sec. V. These results are analyzed in light of both the proposed reaction mechanism, as well as other possible mechanisms. A calibrated value for the reaction rate constant is determined, and possible implications regarding isotope separation and stratospheric chemistry are also mentioned. In Sec. VI the wavelength dependence of the reaction is analyzed using a statistical theoretical model, including both collisional relaxation phenomena of the reactants and RRK unimolecular reaction theory.

II. THE LASER STIMULATED REACTION

A. The NO_2–CO thermal reaction

Calhoun and Crist[3] and Brown and Crist[4] were the first to observe and analyze the kinetics of the thermal reaction

$$NO_2 + CO \rightarrow NO + CO_2 \ .$$

More recent analysis has been performed by Johnston, Bonner, and Wilson[5] and by Thomas and Woodman.[6] All three investigating teams observed this reaction only at elevated temperatures $T \gtrsim 600\,^\circ$K with no observable rate at room temperature. The reaction was found to be bimolecular, being first order in both reactants. In addition, the investigators concluded that there were no intermediate steps involved in the reaction, i.e., the reaction mechanism appeared to be identical to the above stoichiometric equation.

Employing an Arrhenius law fit Crist and co-workers and Thomas and Woodman determined an activation energy $E_{act} = 1.21$ eV and a pre-exponential factor $A = 8.0 \times 10^{-13}$ cc/molecule sec. Johnston *et al.* measured a slightly higher energy barrier to reaction of 1.37 eV and a larger pre-exponential factor of 2.0×10^{-11} cc/molecule sec. Using the room temperature NO_2–CO collision frequency rate of 2.6×10^{-10} cc/molecule sec this data implies a steric factor of from 15 to 300, depending on whose results are employed. Crist's data predicts that in an initial mixture of 1 torr of each of the NO_2 and CO reactants 6.7 mtorr CO_2 is produced per h at 600 °K, 6.2×10^{-2} mtorr/h at 500 °K, and only 1.5×10^{-10} mtorr/h at room temperature (293 °K).

B. Motivation for laser-stimulated reaction study

A study of the laser enhanced NO_2^*–CO reaction is attractive for several reasons. Possible applications to

[a]Work supported by Air Force Cambridge Research Laboratories and National Science Foundation.
[b]Present address: Physics Department—O Group, Lawrence Livermore Laboratory, Livermore, CA 94550.
[c]Present address: Allied Chemical Corporation, Morristown, NJ 07960.

 0021-9606/78/6803-1070$01.00

isotope separation and to solar-radiation-assisted stratospheric chemistry are of interest and will be discussed in more detail in a later section. More importantly, if both the thermal reaction and the reaction of electronically excited NO_2 and CO followed the same energy surfaces, the reaction mechanism of the laser-stimulated reaction would be particularly interesting and simple to unravel.

The activation energy of the thermal reaction is quite large and suggests typical electronic energies in NO_2. Direct one-photon vibrational excitation of the reactants would do little to enhance the rate of reaction because the energy deposited per molecule, about 0.2 eV, would be much smaller than the activation energy.

At present many of the details of the structure of the lowest-lying electronic states of NO_2, and of its associated visible absorption spectrum, are poorly understood.[7] In fact, due to the large density of levels and to perturbations the room temperature NO_2 absorption spectrum remains an unresolved quasicontinuum. The lowest excited electronic state of CO, the $a\ ^3\Pi_r$ at 6.04 eV, is too high to be excited by the optical photons employed in this study, and therefore need not be further considered. In its ground state $\tilde{X}(^2A_1)$, NO_2 is symmetric and bent. The *ab initio* calculations by Gillispie *et al.*[8] predict three low-lying excited doublet levels $^2B_2$ at 1.18 eV, $^2B_1$ at 1.66 eV, and $^2A_2$ at 1.84 eV (with stated accuracy of ± 0.3 eV). Most of the absorption oscillator strength is due to the $^2B_2 \leftarrow \tilde{X}(^2A_1)$ transition, with $^2B_1 \leftarrow \tilde{X}(^2A_1)$ becoming relatively more important at shorter wavelengths. $^2A_2 \leftarrow \tilde{X}(^2A_1)$ is electric dipole forbidden, and the existence of the $^2A_2$ state has yet to be definitely confirmed. From analysis of the absorption spectrum Brand and co-workers have determined the energies of the lowest two excited states: 1.48 eV (8364 Å)[9] for $^2B_2$ and 1.83 eV (6783 Å)[10] for $^2B_1$. Since the energy of the $^2B_2$ state approximately coincides with the measured thermal reaction energy barrier, the thermal reaction may proceed along the $NO_2(^2B_2)$ energy surface.

This study is also motivated by the adiabatic correlation of the reactant and product electronic states. The lowest-lying excited electronic state in NO is the $A(^2\Sigma^+)$, which is 5.45 eV (2220 Å) above the ground state $X(^2\Pi)$, while the lowest excited state in CO_2 is the $\tilde{A}\,^1B_2(\Delta_u)$, which is 5.70 eV (2120 Å) above the $\tilde{X}(^1\Sigma_g^+)$ ground state. In this experiment the maximum energy available for the product states is 5.08 eV (plus several $k_B T_{\text{room}} \simeq 0.1$ eV), which is the sum of the reaction exothermicity 2.37 eV and the maximum photon energy used 2.71 eV (for 4579 Å excitation). Therefore, the products are formed in their ground electronic states, with this excess energy distributed among the translational, rotational, and vibrational degrees of freedom of the products. Because an oxygen atom is transferred to the CO in the reaction, the CO_2 asymmetric stretch mode, as well as the symmetric stretch mode, should be heavily excited.[11]

In the absence of detailed experimental or theoretical curves the manner in which the reactant energy surfaces adiabatically correlate to the product ground electronic state surfaces can be examined only qualitatively. It is useful to employ the Wigner–Witmer rules[11] to correlate reactant NO_2 into NO + O and subsequently recombine CO + O to form CO_2. Note that NO_2 does not actually dissociate in this reaction since the wavelengths employed in this study are all longer than 3979 Å, which corresponds to the onset of predissociation in the NO_2 absorption spectrum.

The discussion of Burnelle, May, and Gangi[12] suggests that the $\tilde{X}(^2A_1)$ and $^2B_1$ states are the Renner–Teller split states of $^2\Pi_u$ in linear NO_2. Therefore. in linear NO_2 both of these states correlate to $NO(^2\Pi) + O(^3P)$.[13] Similarly, both $^2B_2$ and $^2A_2$ are derived from linear NO_2 states with $^2\Phi_g$ character and correlate to $NO(^2\Pi) + O(^1D)$.

If both the $NO_2 + CO \rightarrow NO + CO_2$ and the $NO_2 + CO \rightarrow NO + O + CO \rightarrow NO + CO_2$ reactions proceed along the same surface, then since ground state CO and CO_2 are both singlets, electronic spin is conserved only by the NO_2 species correlating to singlet oxygen, i.e., $^2B_2$ and $^2A_2$[14]:

$$CO(X^1\Sigma^+) + O(^3P) \rightarrow CO_2(\tilde{X}^1\Sigma_g^+)\,,$$

$$CO(X^1\Sigma^+) + O(^1D) \rightarrow CO_2(\tilde{X}^1\Sigma_g^+)\,.$$

This suggests that only the $^2B_2$ and $^2A_2$ states lead to reaction.

Several points should be emphasized in discussing these energy surface correlations. In this presentation the reaction is considered in terms of a virtual process in which an oxygen atom is transferred from NO_2 to CO. Instead, direct correlation of the electronic states of bent NO_2 with CO to the products suggests that all four NO_2 electronic states may lead to reaction. Alternatively, correlation via C_s dissociation (totally unsymmetric) of NO_2 (instead of $D_{\infty h}$ dissociation of linear NO_2)[13] implies that all four NO_2 states correlate to $O(^3P)$. The reaction correlation first discussed is physically the most realistic. In addition, there may be several pathways for reaction—one via the ground state and one via an NO_2 excited electronic state. While the former may be important in the thermal studies, the latter may dominate in this study. Also, though only the $^2B_2$ and $^2A_2$ states may lead to reaction, there may still be a nonzero activation energy for reaction even within these states. It should also be noted that the spectroscopic studies of NO_2 indicate that these states are perturbed and therefore these Born–Oppenheimer states are not true eigenstates.

The only previous photochemical study similar to the one under study was performed by Cohen and Heicklen,[15] who excited NO to the $^2\Sigma^+$ state with 2144 and 2265 Å from a cadmium arc lamp and observed the reaction of this excited electronic state of NO with CO_2 to form NO_2 and CO. This is not the reverse reaction analog of the reaction studied here because the energy surfaces traversed in their reaction are not energetically accessible in this study.

C. The proposed laser-initiated reaction mechanism

The discussion of the previous section suggests that excitation of NO_2 to $^2B_2$ (or $^2A_2$) should accelerate the

TABLE I. Proposed reaction mechanism.

	Rate constant
(1) $NO_2 + h\nu \rightarrow NO_2^*$	$\alpha I/\hbar\omega$[a]
(2) $NO_2^* \rightarrow NO_2 + h\nu$	γ_{rad}
(3) $NO_2^* + CO \rightarrow NO + CO_2$	k_R
(4) $NO_2^* + NO_2 \rightarrow 2NO + O_2$	k_R'
(5) $NO_2^* + CO \rightarrow NO_2 + CO$	γ_{CO}
(6) $NO_2^* + NO_2 \rightarrow NO_2 + NO_2$	γ_{NO_2}

[a] α is the absorption coefficient. This expression assumes that the sample is optically thin.

NO_2–CO reaction. Since throughout the visible wavelength region the absorption spectrum of NO_2 is an unresolved quasicontinuum, all nine wavelengths available from an argon-ion laser [$\lambda = 4545$–5145 Å, $\alpha = 0.005$–0.02 (cm torr)$^{-1}$ (the low resolution absorption coefficient)] and radiation from an argon-ion laser-pumped Rhodamine 6G dye laser [5700–6400 Å, $\alpha = 0.001$–0.002 (cm torr)$^{-1}$] are readily absorbed. With the exception of the 4545 Å argon ion laser line,[16] which is not employed, all the mentioned wavelengths excite $^2B_2$ states. Therefore, excitation by the cw visible radiation promotes NO_2 to $^2B_2$ which should then react with CO. $^2A_2$ cannot be populated by one-photon absorption from the ground state; however, it may be produced by collisions.

The proposed reaction mechanism is displayed in Table I in which I represents the visible laser intensity and $\hbar\omega$ is the visible photon energy. NO_2^* denotes reactive NO_2, be it the laser excited levels in the $^2B_2$ state or any other reactive state above the reaction energy barrier (within either this or another electronic state). In this mechanism ground state NO_2 absorbs a single visible photon and is excited to $^2B_2$. Loss of excitation may occur via reaction with NO_2 or CO, by spontaneous emission, diffusion to the walls (not listed in the table), or collisional deactivation by NO_2 or CO. Typical collisional decay times of ~100 nsec at 1 torr[17,18] are much faster than either radiative decay (~70 μsec)[18,19] or diffusion, and therefore these last two processes may be neglected. The role of Reaction (4) is considered below.

Treating NO_2^* as a steady state intermediate the rate law for CO_2 production is

$$\frac{d[CO_2]}{dt} = k_R\left(\frac{\alpha I}{\hbar\omega}\right)\frac{[NO_2][CO]}{\gamma_{CO}[CO] + \gamma_{NO_2}[NO_2]} \quad . \tag{1}$$

This assumes that collisional deactivation is much faster than NO_2^* depletion by either reactive channel, an assumption that is borne out by the experimental results. The above prediction is compared to experimental data in Sec. V. In addition, alternate mechanisms in which either an NO_3 intermediate or vibrationally hot CO play an important role in the reaction are also considered there.

The actual collisional deactivation scheme is much more involved than the simple picture painted above. Since $^2B_2$ and $\tilde{X}(^2A_1)$ are spectroscopically mixed, they are probably also strongly coupled by collisions. Relaxation of fluorescing $^2B_2$ states appears to be by multiple collisions, each involving the loss of vibrational quanta in the collisionally populated $\tilde{X}(^2A_1)$ state with near gas-kinetic rate. Therefore, at the experimental pressures of several torr the laser-excited levels of $^2B_2$ are populated along with some of the high-lying vibrational levels of $\tilde{X}(^2A_1)$, and possibly also some $^2B_1$ and $^2A_2$ levels. The details of collisional deactivation are reconsidered in Sec. VI.

It should be pointed out that if $\gamma_{CO}/\gamma_{NO_2}$ is independent of the actual NO_2 level that is being relaxed, the pressure dependence of this simple mechanism is identical to one employing a more detailed deactivation mechanism in which the various collisionally populated NO_2 states may have different reaction cross sections. In fact, in a low resolution analysis of $NO_2(^2B_2)$ visible fluorescence in argon Myers *et al.*[20] found $\gamma_{Ar}/\gamma_{NO_2}$ to be fairly independent of the wavelength of the fluorescence, thus reinforcing this approximation. This has been confirmed for $NO_2(^2B_2)$ in CO by the authors. Since the $^2B_2$ state is responsible for visible fluorescence and is also thought to be responsible for reaction, these arguments relating relaxation in these two different processes are justified.

The effects of laser heating of the medium must also be estimated. The visible laser, with power P, may be modeled as having a uniform cross section of radius a. It is centered in a cylindrical cell, with radius b, with NO_2 density n, and an effective thermal conductivity K. If the cell walls are fixed at room temperature, the maximum rise in temperature above ambient ΔT clearly occurs in the center of the cell, and is given by[21]

$$\Delta T = \frac{\alpha n P}{4\pi K}\left(1 + 2\ln\frac{b}{a}\right) \quad . \tag{2}$$

For the conditions of this experiment, say 800 mW of 4880 Å incident on 2 torr NO_2 and 4 torr CO, $\alpha = 0.01$ (cm torr)$^{-1}$, $K = 3\times10^3$ erg/sec cm °C, and $b/a = 4.5$, one obtains $\Delta T = 16$ °C. Clearly, this rise in gas temperature is much too small to influence either the forward NO_2–CO thermal reaction or the endothermic back reaction.

Though thermal decomposition of NO_2 at room temperature is insignificant, photodecomposition [Reaction (4) in Table I] is quite important. Creel and Ross[22] reported that $k_R' = 4.2\times10^{-14}$ cc/molecule sec with 4880 Å excitation, corresponding to reaction in one out of every 5000 NO_2^*–NO_2 collisions. Since the rate measured in this experiment is slower, the NO_2^*–NO_2 reaction sets an upper limit for the period of irradiation in which the initial reactant concentration remains unchanged. Another consequence of this reaction is that, unless a great over pressure of CO is employed, the extent of the NO_2^*–CO reaction can be determined reliably only by detection of the CO_2 product, as NO is produced in both reactions. It should also be noted that three-body thermal recombination of the NO and O_2 products is extremely slow under experimental conditions.[22]

The CO_2 produced in the laser-induced reaction is not expected to react further with any of the products or re-

actants. Collisions of NO_2 or NO_2^* with NO or O_2 may lead to isotopic exchange; however, no new products are expected. The rates of thermal reaction of CO with either O_2[23] or NO[24] are much slower than the NO_2–CO thermal reaction, and therefore may also be ignored. At 2 torr pressure only 4% of all NO_2 exists as the dimer N_2O_4.[25] Since this concentration is very small and because N_2O_4 does not absorb in the visible, N_2O_4 does not influence the reaction.

III. EXPERIMENTAL APPARATUS

Briefly, a typical experiment proceeded as follows: After purifying the NO_2 and CO, each having a partial pressure of a few torr, the reactants were allowed to mix in the reaction cell. After irradiation the CO_2 product (~1 mtorr) was distilled and transferred to the detection cell. The CO_2 was then mixed with 850 mtorr of argon and measured by laser-induced fluorescence, as is detailed in the next section.

An extensive Pyrex gas handling system, capable of thorough distillation and purification, formed the bulk of the experimental equipment. The gas handling manifold consisted of a vacuum pump station, gas storage area, a reaction and a detection cell, along with associated coldfingers and cold traps. Only Pyrex and stainless steel tubing, along with stainless steel bellows valves and Teflon-FETFE O-ring stemmed stopcocks (Ace Glass Company), were employed. Oilfree cryo-vac-sorb pumps (to 1/3 mtorr) and sputter-ion pumps (to $< 10^{-7}$ torr) were used to evacuate the cells. Such precautions were necessary in choosing the apparatus components for if NO_2 were to attack the wall materials or were to react with oil from standard mechanical or oil-based diffusion pumps, large amounts of the laser-stimulated reaction products NO and CO_2 would form. A pirani gage and a stainless steel capacitance manometer, calibrated by a McLeod gauge, were employed to measure the reactant concentrations.

Only gases of the highest available purity were used in this experiment, the CO being 99.99% research purity grade, with a stated maximum CO_2 impurity of 10 ppm, and the NO_2 being 99.5% pure. The CO and NO_2 were stored in separate activated alumina-filled U tubes to remove water vapor, nickel carbonyl (from the CO), and other heavy contaminants. In addition, the NO_2 U tube was encased in aluminum foil to prevent photodecomposition by room lighting.

Prior to use CO was purified by transfer to a liquid-nitrogen-cooled cold trap in order to freeze out any CO_2 contaminant. NO_2 samples obtained directly from the gas cylinder froze to a deep blue condensate. This indicated the presence of N_2O_3, whereas pure NO_2 instead condenses to colorless N_2O_4 crystals. The N_2O_3 molecule is unstable in the gas phase but forms a stable (liquid and solid) condensate when both NO_2 and NO are present. The NO_2 was freed of the NO, as well as of other more volatile contaminants, by a freeze–pump–thaw cycle at $T = -197\,^{\circ}C$ (liquid nitrogen) followed by three such cycles at $T \simeq -80\,^{\circ}C$ (cooled acetone bath); after this distillation the frozen crystals were colorless. CO_2 impurities have been detected in industrially supplied NO_2.[26] This purification procedure would also eliminate any such impurity in the NO_2.

The cylindrical Pyrex reaction cell was of 9.1 cm average length with a 1.9 cm inside diameter. Pyrex windows were fused at Brewster's angle at either end, corresponding to the vertical polarization of the incident visible laser. The laser was aligned through the center of the cell through a fixed aperture. A Scientech #362 thermopile power meter was employed to monitor laser stability and to measure the power absorbed by the reacting mixture. It was frequently calibrated by sending known currents through the meter head, thereby yielding consistent relative readings with precision ±1% for the visible lasers and ±3% for the CO_2 laser. The estimated absolute accuracy was ±10%.

The detection cell was a 6 cm long, 1.1 cm inside diameter Pyrex cylinder with BaF_2 windows attached at either end at Brewster's angle with red wax (Cenco). A sapphire window was located on top of the cell to permit observation of the CO_2 laser induced fluorescence by a liquid-nitrogen-cooled InSb photovoltaic detector loaded by a 7 KΩ resistor. As is discussed in the next section this window–detector combination affords double protection against observation of CO_2 laser 10.6 μ scatter amidst the 4.3 μ fluorescence signal because sapphire is opaque, and the responsivity of the InSb detector is very small for $\lambda > 5.5$ μ.

Since the volumes of the reaction and detection cells must be known in order to determine the absolute reaction rate, they were measured by volume comparison with a premeasured reference cell.

A 4 W commercial argon-ion laser provided multimode cw radiation at nine wavelengths between 4545 and 5145 Å for the reaction studies. This laser was also used to pump a cw commercial Rhodamine 6G jet stream dye laser,[27] which provided over 500 mW of tunable radiation from 5750–6200 Å with a 1 Å linewidth. For the CO_2 laser-induced fluorescence detection a homemade grating-tuned cw CO_2 laser was employed, which could provide over 10 W of TEM_{00}, stable single-rotational line radiation in either the 9.4 or 10.4 μ band.

IV. MEASUREMENT OF THE CO_2 PRODUCT

The technique of CO_2 detection by laser-induced fluorescence (LIF) is easily understood by reference to Fig. 1. Radiation from a CO_2 laser is resonant with one of the $(10^00) \rightarrow (00^01)$ 10.4 μ band or $(02^00) \rightarrow (00^01)$ 9.4 μ band rotational transitions in molecules in proper Doppler velocity resonance, thereby causing a transition to (00^01). Once in (00^01) the molecule may fluoresce a 4.3 μ photon and thereby relax to (00^00). Alternatively, it may relax by diffusion to and relaxation by the cell walls or by molecular collisions. Radiative decay to (10^00) or (02^00) are both 2000 times less probable than emission to the ground state.[28]

In this study the $P(16)$, $\lambda = 10.55$ μ laser line was used to induce the transition (10^00), $J = 16 \rightarrow (00^01)$, $J = 15$. This line was chosen because of the higher available laser power compared to the analogous 9.4 μ line and because the absorption coefficient is higher than for

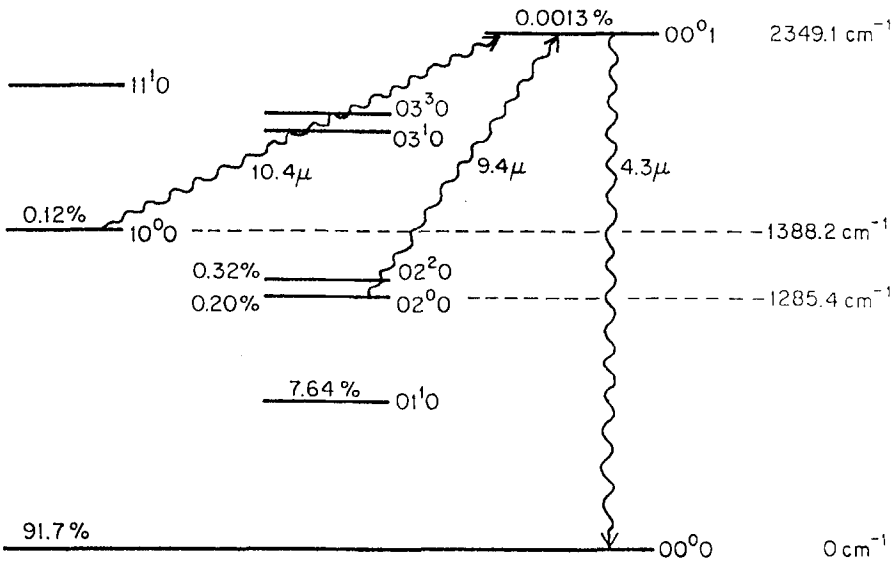

FIG. 1. The CO_2 vibrational level structure with room temperature fractional thermal populations of relevant levels.

other possible rotational transitions. The unfocused CO_2 laser (3 W) was mechanically chopped at 338 Hz and was aligned through a fixed aperture before impinging on the detection cell. The 4.3 μ fluorescence was collected with $f/4$ optics and was detected by a liquid-nitrogen-cooled InSb photovoltaic element; the observed signal was then obtained by lock-in detection.

This fluorescence system is sensitive from 1.0 to 5.5 μ, as determined by both the InSb sensitivity and the transmission characteristics of the sapphire window preceding it. Because of this broad-band response, not only is the (00^01), $J=15 \rightarrow (00^00)$, $J=14, 16$ fluorescence observed but also that from collisionally coupled rotational levels (00^01), $J \neq 15$. In addition, fluorescence is detected from collisionally excited combination bands, such as $(01^11) \rightarrow (01^10) + h\nu$, which also emit in the 4–5 μ range.

The addition of a fixed buffer pressure of argon (p_{Ar} = 850 mtorr) to the CO_2 was found to increase sensitivity by over an order of magnitude for the typical CO_2 pressures produced by the reaction of $p_{CO_2} \cong 1$ mtorr. The argon inhibits the diffusion of CO_2 (00^01) to the walls, while relaxing it only very slowly, thereby allowing more of the excited molecules to fluoresce. Details of the fluorescence kinetics may be found in Appendix A. Also, with such a buffer present the fluorescence intensity is linearly proportional to p_{CO_2} since only the concentration of absorbing molecules is important in the kinetics as all nonradiative relaxation rates are determined by the the fixed amount of buffer (for $p_{Ar} \gg p_{CO_2}$) (see Appendix A). This was confirmed in a calibration run at typical experimental conditions with known amounts of CO_2 in 850 mtorr Ar, as depicted in Fig. 2, in which 100 nV corresponded to 3.1 mtorr CO_2 in the detection cell and and to 0.7 mtorr in the reaction cell. Because of this linearity the calibration can be extended to very low concentrations of CO_2. Another merit of this method is that small amounts of impurities, say due to incomplete distillation or unexpected reaction products, will not affect the calibration as long as the impurities are not resonant with the laser.

All detection work was performed at an ambient temperature maintained at 19.7 ± 0.5 °C because the thermal population of (10^00), and therefore also the fluorescence intensity, increases by +2.3% per °C. The increase in gas temperature due to CO_2 laser absorption is easily estimated using Eq. (2) to be negligible ($\simeq 10^{-2}$ °C).

V. EXPERIMENTAL RESULTS AND IMPLICATIONS

A. Procedure

Because each experimental run required several hours, extreme care was exercised to maintain identical conditions for each trial. All work was performed in a completely darkened room to prevent NO_2 photodecomposition and background NO_2–CO photochemical reactions.

After purification the reactants were allowed to thoroughly mix in the reaction cell and were then irradiated. Typical irradiation times were from 15 min (argon-ion laser lines) to 2 h (Rhodamine 6G dye laser wavelengths). To compensate for laser power drift and NO_2 photodecomposition the laser power transmitted

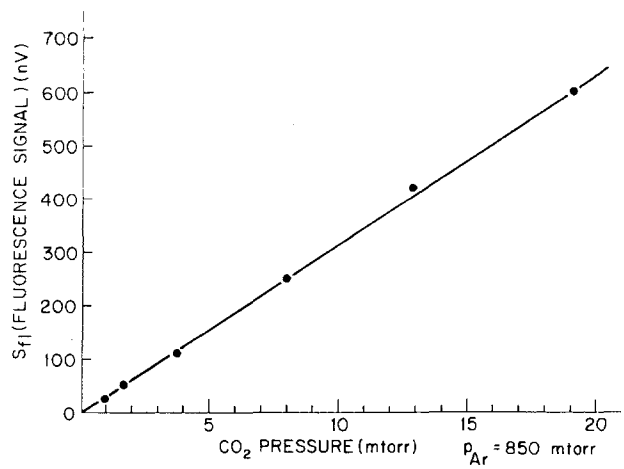

FIG. 2. Calibration of 4.3 μ fluorescence vs p_{CO_2} with p_{Ar} = 850 mtorr.

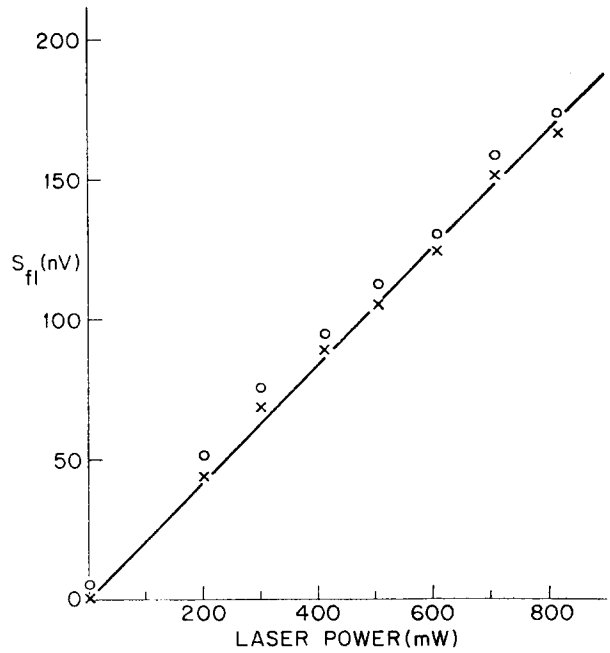

FIG. 3. Fluorescence intensity of reaction-produced CO_2 as a function of incident visible laser power.

through the cell was carefully monitored during the reaction. After irradiation NO_2, CO_2, and N_2O_3, the latter due mostly to the NO formed in the $NO_2^*-NO_2$ reaction, were collected in a liquid-nitrogen-cooled coldinger. The remaining gases CO and O_2, the O_2 also from the $NO_2^*-NO_2$ reaction, were pumped out. The NO and NO_2 were then transferred to another coldfinger immersed in an n-propanol slush, $T \simeq -127\,^\circ$C, leaving CO_2 in the gas phase. The CO_2 was then transferred to the detection cell, mixed with argon, and was then detected by LIF. Since the NO, NO_2 collecting coldfinger occupied only 4% of the relevant volume, 96% of the created CO_2 was retained in this distillation, neglecting wall adsorption effects.

Several null runs were performed in which the same procedures were followed as during a run, with the exception that the samples were not excited during the "laser-irradiation" cycle. A 15 min "irradiation period" null run, with $p_{NO_2} = 2$ torr and $p_{CO} = 4$ torr, produced a background signal of ~7 nV, while a 2 h null run led to ~20 nV. Therefore, this background signal was very small in comparison to typical 15 min long argon-ion laser excitation signals of ~100 nV, but was not insignificant compared with the results of dye laser excitation, which led to about 70 nV in 2 h. This background signal was neither due to thermal reactions nor to laser heating, but rather to the reaction of NO_2 with the apparatus. In the experimental plots to follow raw data is plotted as circles, whereas "corrected" data, in which the background has been subtracted from the raw data, appears as X's.

The rate of CO_2 production was found to be linear with the duration of irradiation, measured up to 15 min (with 800 mW incident on 2 torr NO_2 and 4 torr CO). This indicates that the reaction does not depend on the appearance of any of the products of either the NO_2^*-CO, $NO_2^*-NO_2$, or any NO_2–apparatus reactions.

B. Dependence on laser intensity

Figure 3 depicts the variation of the quantity of CO_2 produced, as determined by the fluorescence signal S_{fl} with incident visible laser power P (4880 Å, $p_{NO_2} = 2$ torr, $p_{CO} = 4$ torr). The laser power was varied from 0 to 800 mW with constant beam spot size, corresponding to an intensity change of 0–30 W/cm^2. Since this plot may need to be corrected from run-to-run variations in absorption length due to variations in laser alignment through the cell, the loss of NO_2 due to photodecomposition, and laser saturation, each contribution should be analyzed. The absorption length variations were estimated to be at most 3%, and the maximum loss of NO_2 due to the $NO_2^*-NO_2$ reaction was estimated to be $\simeq 6\%$ at 800 mW by observing the rate of O_2 formation in irradiated pure NO_2.[22] At the NO_2 pressures of interest (1–4 torr) no laser saturation effects were observed. Therefore, these corrections appear to be unimportant. Also, the NO_2 absorption coefficient was found to be independent of the CO pressure. This observation is expected since the NO_2 Doppler width of 1 GHz is much larger than anticipated CO pressure broadening ($\simeq 100$ MHz), and also since the Doppler profiles of adjacent optical transitions in NO_2 overlap.

Figure 3 is well described by a straight line. This linearity is in agreement with the proposed reaction mechanism described by Eq. (1). The lack of upward curvature discounts the importance of multiphoton effects in the intensity regime under study. In addition, this figure further proves that the reaction is nonthermal because, if thermal effects dominated, the plot would increase exponentially with laser power since the temperature in the Arrhenius equation is linear in the laser power.

C. Dependence on reactant concentrations

Equation (1) predicts the expected dependence on reactant concentration in the proposed mechanism. This behavior is more easily analyzed by examining the reciprocal of the equation, which implies that

$$\frac{1}{[CO_2]_{formed}} \propto \frac{1}{S_{fl}} \propto \frac{\gamma_{CO}}{[NO_2]} + \frac{\gamma_{NO_2}}{[CO]} \quad . \tag{3}$$

Therefore, this mechanism suggests that $1/S_{fl}$ is linear with either $1/[NO_2]$ or $1/[CO]$, with [CO] or $[NO_2]$ fixed, respectively. Since Eqs. (1) and (3) assume an optically thin absorption cell, and since under experimental conditions $\alpha l = 0.1-0.3$ (l = path length), this assumption is not strictly true and some correction is necessary. Therefore, the data is plotted as P_{abs}/S_{fl} vs $1/[CO]$ with $[NO_2] = 2$ torr in Fig. 4 and as $1/S_{fl} \times (P_{abs}/[NO_2])$ vs $1/[NO_2]$ with $[CO] = 3.5$ torr in Fig. 5, where P_{abs} is the average absorbed power during the run. Plotted in such a manner the data does indeed appear linear, indicating agreement with the proposed mechanism.

The values of $\gamma_{CO}/\gamma_{NO_2}$ obtained from these two plots are 0.55 ± 0.1 and 1.2 ± 0.3, respectively. Since the data

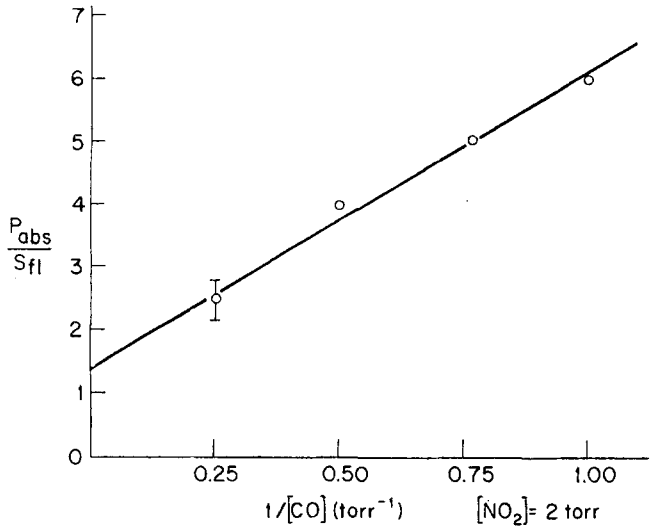

FIG. 4. Plot of inverse of S_{fl}, multiplied by the absorbed power, as a function of 1/[CO], for $[NO_2] = 2$ torr.

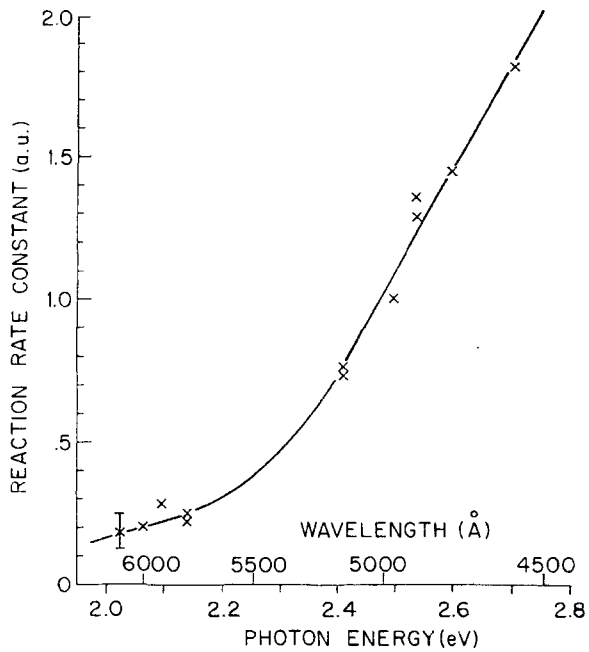

FIG. 6. Variation of the normalized reaction rate constant, determined by laser-induced fluorescence of the CO_2 product, as a function of the exciting visible photon energy.

are plotted in an inverse manner, small variations in data, as well as small corrections due to the background, can induce large changes in this ratio while maintaining the linearity of the data. It is interesting to note that the ratio of CO and NO_2 visible fluorescence-quenching efficiency has been measured by the authors to be $\simeq 0.6$.[2]

D. Variation of the reaction rate with exciting wavelength

The reaction dynamics of this photochemical reaction were further investigated by varying the wavelength of excitation. The relative effective reaction rate constant k_R obtained in this study is plotted vs the exciting wavelength (4579–6125 Å) in Fig. 6. This plotted rate constant was obtained by dividing the observed S_{fl} both by the average absorbed laser power and by the duration of irradiation. Therefore, the data is normalized for the different available laser power at each wavelength, the wavelength-dependent absorption coefficient, the different lengths of irradiation, and for the small amounts of NO_2 photodecomposition. Since the rate of reaction is linear in laser intensity, the maximum available laser power was employed at each wavelength. The plotted data has also been corrected for the background formation of CO_2. By multiplying the ordinate at each wavelength by the photon energy (or by $1/\lambda$) the relative quantum yield may be obtained; it behaves qualitatively the same as k_R.

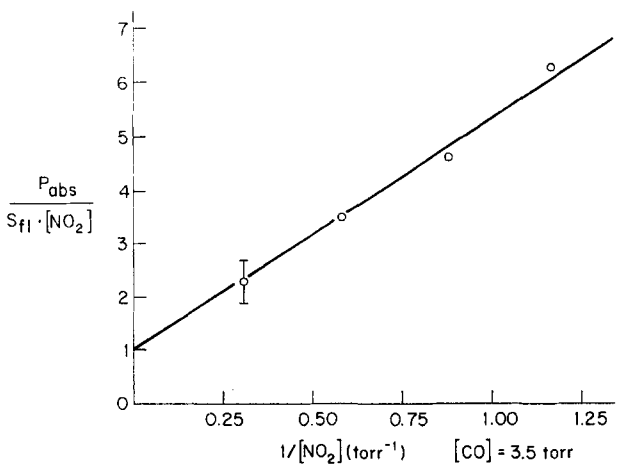

FIG. 5. Plot of inverse of S_{fl}, normalized by the $P_{abs}/[NO_2]$ factor, as a function of $1/[NO_2]$, for $[CO] = 3.5$ torr.

Whereas in argon-ion laser excitation runs ($\lambda = 4579$, 4765, 4880, 4965, and 5145 Å) the irradiation time was 15 min, the dye laser ($\lambda = 5785$, 5920, 6002, and 6125 Å) excitation times were much longer (2 h) because of the relatively small absorption coefficient and the small reaction rate constant. In fact, to enhance dye laser absorption the beam transmitted through the sample was once again reflected through the cell. These particular listed dye laser wavelengths were chosen because they represent relative maxima in the NO_2 absorption coefficient.

The effective reaction constant increases by a factor of 10 as the wavelength decreases from 6125 to 4579 Å, corresponding to an increase in photon energy from 2.02 to 2.71 eV. Because of collisional redistribution of energy, the observed curve is smooth, with no apparent structure. In fact, a very similar wavelength dependence was observed by Creel and Ross[22] in their study of $NO_2^* + NO_2 \rightarrow 2NO + O_2$. Employing the RRK model described in Sec. VI the activation energy appears to be about 1.8 ± 0.2 eV, or about 0.3–0.7 eV higher than the thermal activation energy. Unfortunately, because of the relatively large error bars at the longer wavelength data and the absence of data at even longer wavelengths, it is not certain whether the laser-stimulated reaction energy barrier is in fact higher than the thermal value, or whether the difference is an experimental artifact. It is interesting to note that the measured E_{act} is, in fact,

more nearly equal to the $^2B_1$ and $^2A_2$ energies than to that of $^2B_2$. Even if only $NO_2(^2B_2)$ reacts with CO, these results indicate that a small amount (0.1 to 0.5 eV) of vibrational and/or translational energy is still required to cross the reaction barrier in this state.

The calculation in the next section indicates that whereas collisions are efficient in relaxing NO_2^*, only about one in every 10^5 collisions of NO_2^* and CO are reactive. Since collisions, and neither the reaction nor spontaneous emission, dominates the dynamics of NO_2^*, it is a steady-state nonequilibrium distribution of NO_2^* that is available for reaction. Because of this collisional coupling, not only directly laser-excited (and collisionally induced) $^2B_2$ states, but also the high-lying vibrational levels of $\tilde{X}(^2A_1)$, and possibly also $^2A_2$ and $^2B_1$, are populated.

In the next section the effects of collisional relaxation and reaction dynamics on the wavelength dependence portrayed in Fig. 6 are discussed quantitatively. The shape of the observed curve, however, may be described qualitatively. The observed reaction rate constant at a given energy depends on the population of each level and on each level's reactivity. There are three contributions to the overall observed increase of reactivity with energy. The first is merely the increase in reactivity with energy due to a more favorable statistical distribution of energy or due to dynamical effects. The other two effects depend on collisional relaxation. Since NO_2^* is relaxed by a multistep process, the higher a photon excites a particular molecule above the activation energy the more collisions are required to relax it to an energy below the barrier. At shorter wavelengths the effective relaxation rate is slower, and therefore the observed reaction rate constant is larger. Finally, since collisional relaxation involves both $^2B_2$ and $\tilde{X}(^2A_1)$, the relative density of states of $^2B_2$ to $\tilde{X}(^2A_1)$ increases as the energy increases. If $^2B_2$, and not $\tilde{X}(^2A_1)$, is the reactive species, this would also contribute to the observed k_R behavior.

E. Determination of k_R and subsequent implications

A calibrated value for k_R may be obtained by rewriting Eq. (1) as

$$\frac{k_R}{\gamma_{NO_2}} = \frac{[CO_2]VF}{T} \frac{[NO_2] + \frac{\gamma_{CO}}{\gamma_{NO_2}}[CO]}{[CO]} \frac{\hbar\omega}{P_{abs}} , \qquad (4)$$

where $[CO_2]$ is the final CO_2 concentration produced in a time T in a volume V and where $F = 1.04$ compensates for the loss of CO_2 due to distillation. Using $\gamma_{CO}/\gamma_{NO_2} = 0.6$ the result $k_R/\gamma_{NO_2} = 2.1\times10^{-5}$ is obtained at 4880 Å, indicating that the rate of reaction is indeed much slower than the rate of collisional transfer. The value obtained for k_R/γ_{NO_2} has an estimated 40% accuracy, which includes experimental uncertainties and allowance for some variation $\gamma_{CO}/\gamma_{NO_2}$. The quantum yield ϕ is defined as

$$\phi = \frac{\#\text{ of } CO_2 \text{ molecules produced}}{\#\text{ of photons absorbed}}$$

and may be evaluated for 4880 Å ($p_{NO_2} = 1.7$ torr, $p_{CO} = 3.5$ torr) by noting that it is equivalent to the product of the first and third terms of Eq. (4); this leads to $\phi = 1.7\times10^{-5}$.

While the value obtained for k_R/γ_{NO_2} is basically an experimentally determined quantity, the value obtained for k_R depends on previously measured values for γ_{NO_2} and the exact nature of collisional deactivation. Sakurai and Broida[17] analyzed the kinetics of NO_2^* visible fluorescence excited by 4880 Å from an argon-ion laser. They observed a fluorescence spectrum consisting of a series of lines superimposed upon a broad unresolved quasicontinuum which extended from the exciting wavelength to at least the long wavelength cutoff of their photomultiplier (~7500 Å). The line spectrum is due to transitions from the laser-excited $^2B_2$ states to various rotational and vibrational states in the ground state, while the quasicontinuum is due to transitions from collisionally populated $^2B_2$ levels to $\tilde{X}(^2A_1)$.

By varying the NO_2 pressure Sakurai and Broida were able to determine the value of $\sigma^2\tau$ for various features of the fluorescence, where σ is the appropriate collision diameter and τ is the apparent pressure-independent lifetime. In their fluorescence cell the transit time of NO_2^* to the walls (in the Knudsen pressure regime) was about 45 μsec, whereas the "bulk"[29] radiative lifetime was somewhat longer (~75 μsec).[18,19] Combining both contributions τ is actually 28 μsec. Using this value of τ one may ascertain that (1) the laser excited $^2B_2$ states decay with a rate constant of 4.1×10^{-10} cc/molecule sec, (2) the visible fluorescence integrated from 5050–5070 Å is quenched with a rate constant of 1.5×10^{-10} cc/molecule sec, and (3) the continuum fluorescence integrated from 4880 to about 7500 Å deactivates with a rate constant of 2.7×10^{-11} cc/molecule sec. These relaxation rates correspond to 0.57, 1.5, and 8.3 gas-kinetic collisions, respectively, and imply that under experimental conditions only 3×10^{-6} of all NO_2 molecules are excited.

These three relaxation rates describe the quenching of different NO_2^* states. In the model proposed in the next section it is the first rate that most nearly describes the vibrational level-to-vibrational level relaxation in NO_2^*. It can easily be shown that this model is numerically equivalent to a simpler model in which k_R, on the left-hand side of Eq. (4), represents the average reactivity of only the states at the exciting wavelength. γ_{NO_2} then represents an effective relaxation rate slower than the first rate quoted above and numerically more equal to the second. Using this second rate, at 4880 Å, $k_R = 3.2\times10^{-15}$ cc/molecule sec, implying that only one in every 80 000 collisions of NO_2^* with CO is reactive. (Employing the first rate leads to $k_R = 8.6\times10^{-15}$ cc/molecule sec or 30 000 collisions, while the last one implies $k_R = 5.7\times10^{-16}$ cc/molecule sec or 450 000 collisions.)

The relaxation and reaction rates reported in this paper are 2.5 times those reported in the initial communication[2] of these results because in the earlier letter the pressure-independent NO_2^* lifetime was equated to the radiative lifetime, with no allowance made for trans-

it to the walls. These quoted NO_2^* deactivation rates are now in good agreement with those determined by Schwartz and Johnston.[18]

In collisions NO_2^* both loses energy and redistributes energy among nearly isoenergetic states. Therefore, this reported value for k_R represents the average of the reaction rate constants of those populated states near 2.54 eV (4880 Å). It is very surprising that even though all participating NO_2^* molecules have energy far in excess of the NO_2–CO activation energy, only one in every 80 000 collisions is reactive. The following four effects may account for this behavior: (1) The reactive NO_2^* population may be diluted into a dense manifold of nonreactive states, (2) some internal excitation of CO may be necessary to promote the reaction, (3) there may be a translational energy barrier even when the reactants are internally excited, and (4) steric factors may be important.

If the energy is collisionally equilibrated among isoenergetic $^2B_2$ and $\tilde{X}(^2A_1)$ states, only 10%–25% of the energy remains in $^2B_2$. If either $^2B_1$ or $^2A_2$ were involved in the reaction dynamics, the relative density of states factor would be even much smaller, again implying that only a small percentage of excited molecules would be in the proper states for reaction. It should also be noted that the $^2B_2$ state is considerably more bent (equilibrium bond angle = 102°)[8] than the ground state (134°) and that the visible laser predominantly excites the high bending modes of $^2B_2$. These highly bent levels may not be as reactive as the more linear $^2B_2$ states, corresponding to stretching mode excitation. It is possible that the observed reactivity is due to the partial relaxation of the laser-excited $^2B_2$ states into these reactive levels.

The relative orientation of the reactant molecules may also play a very important role in the laser-stimulated reaction. In the associated thermal reaction the steric factor was measured to be 15–300.[3–6] Since reaction probably occurs in a staggered ("W" shaped) O–N–O–C–O configuration,[30] and since the laser excites a highly bent state, the relatively small observed reaction rate may simply be due, in part, to rigid orientation requirements. It should be emphasized that though the measured rate appears to be slow, it is still much faster than that of the associated thermal reaction at room temperature in which only one in every 10^{24} collisions is reactive.

Isotope separation and the impact on stratospheric chemistry were mentioned as two possible applications of this study in the Introduction. Selective excitation of either $^{15}N^{16}O_2$ or $^{14}N^{16}O^{18}O$ may be feasible in the red or yellow part of the absorption spectrum; however, the rate of reactant isotopic scrambling, such as $^{15}NO_2^* + {}^{14}NO_2 \rightarrow {}^{15}NO_2 + {}^{14}NO_2^*$, is much faster than the observed reaction rate, suggesting little net isotopic selectivity. In addition, any enriched ^{15}NO product, due to either the NO_2^*–CO or the NO_2^*–NO reaction, would have to be separated from NO_2 very rapidly as ^{15}NO and $^{14}NO_2$ readily scramble.[31] The dominant mechanism in O_3 destruction in the stratosphere is catalytic destruction by NO and NO_2.[32] Since NO_2 and CO are both relatively abundant at an altitude of 25 km, the solar-assisted reaction analog of the reaction under study may be of interest in the dynamics involving the overall molecular makeup of the stratosphere. Using the known solar flux, the NO_2 absorption coefficient, k_R determined in this study, and quenching by the ambient atmospheric constituents at 25 torr the effective rate constant k in

$$\frac{d[NO]}{dt} = k[NO_2][CO]$$

is calculated to be only 10^{-24} cc/molecule sec. Though faster than the thermal rate (10^{-39} cc/molecule sec) at stratospheric temperature (225 °K), it is still slow compared to other relevant thermal and photochemical reactions.

TABLE II. Proposed NO_3 laser-initiated reaction mechanism.

	Rate constant
$NO_2 + h\nu \rightarrow NO_2^*$	$\alpha I/\hbar\omega$
$NO_2^* \rightarrow NO_2 + h\nu$	γ_{rad}
$NO_2^* + CO \rightarrow NO + CO_2$	k_R
$NO_2^* + NO_2 \rightarrow NO_3 + NO$	k_1
$NO_2^* + CO \rightarrow NO_3 + C$	k_2
$NO_3 + CO \rightarrow NO_2 + CO_2$	k_3
$NO_3 + NO_2 \rightarrow NO + O_2 + NO_2$	k_4
$NO_3 + CO \rightarrow NO + O_2 + CO$	k_5
$NO_2^* + NO_2 \rightarrow NO_2 + NO_2$	γ_{NO_2}
$NO_2^* + CO \rightarrow NO_2 + CO$	γ_{CO}

F. The reaction mechanism

In Table I of Sec. II.C a laser-initiated reaction mechanism was proposed which has been found to be in agreement with the variations of the experimentally observed rate of reaction vs both laser intensity and reactant concentration. Though it is difficult to "deconvolute" the role of collisions and to determine exactly which NO_2 states are responsible for reaction, the essence of this mechanism is that the CO_2 product is formed only by NO_2^*–CO collisions. In this section two other plausible mechanisms are considered.

1. The NO_3 mechanism

NO_3 is an intermediate that is found in many reactions involving nitrogen oxides and has been suggested as a possible intermediate in the NO_2^*–NO_2 reaction.[22] It is now considered as a possible intermediate in the NO_2^*–CO reaction. A new, "NO_3" hypothetical mechanism is outlined in Table II. NO_2^* may react with CO to form NO and CO_2 as before, or may instead react with NO_2 to form NO_3. The reaction of NO_2^* with CO to form NO_3 + C is about 5 eV endoergic, including the energy contribution from laser excitation, and therefore cannot proceed ($k_2 = 0$). The NO_3 may then either react with CO to form NO_2 and CO_2, or may decompose to NO + O_2 by

collision with NO_2 or CO. The following reasonable assumptions are now made in analyzing the kinetics: (1) NO_2^* and NO_3 maintain steady-state populations, (2) $[NO_2]$, $[CO] \gg [NO_3]$, $[NO_2^*]$, $[NO]$, $[O_2]$, $[CO_2]$, (3) $\gamma_{CO} \gg k_R$, (4) $\gamma_{NO_2} \gg k_1$, and (5) radiative losses are insignificant. This leads to the rate law

$$\frac{d[CO_2]}{dt} = \frac{\frac{\alpha I}{\hbar\omega}[NO_2][CO]}{\gamma_{CO}[CO] + \gamma_{NO_2}[NO_2]} \times \left\{ k_R + \frac{k_1 k_3 [NO_2]}{k_4[NO_2] + (k_3 + k_5)[CO]} \right\} . \quad (5)$$

The originally proposed mechanism corresponds to $k_R \neq 0$, k_1, $k_3 = 0$, while the pathway with the NO_3 reactions dominant has $k_R = 0$, k_1, $k_3 \neq 0$. Both mechanisms have the same dependence on visible laser intensity but have different variation with reactant concentration. On the basis of thermal results[23] it is reasonable to set $k_4 = k_3 + k_5$. In Fig. 7 the calculated $1/S_{f1} (\propto 1/[CO_2])$ is plotted vs $1/[CO]$ at fixed $[NO_2]$ for this NO_3 mechanism (unbroken lines) and for the original mechanism (dashes). Figure 8 displays an analogous calculation for $1/S_{f1}$ vs $1/[NO_2]$ at fixed [CO]. Both plots have been calculated for $\gamma_{CO}/\gamma_{NO_2}$ equal to either 0.6 or 1.0, and the experimental data has also been added to each display. Clearly, the data disagrees with this proposed NO_3 mechanism.

2. The role of vibrationally excited CO

Another possible reactive pathway concerns the reaction of vibrationally hot CO, denoted as $CO^\dagger$, with NO_2. CO may become highly vibrationally excited due to energy transfer from NO_2^* to $v = 1$, followed by rapid CO $V-V$ equilibration, with only very slow decay out of the CO vibrational manifold due to radiative processes, $V-T$ relaxation, and $V-V$ transfer to NO_2. Reaction may occur due to collisions of unexcited NO_2 with CO which has been vibrationally excited to an energy above the NO_2–CO thermal reaction barrier, i.e., $v \geq 5$, or due to collisions of partially excited NO_2, perhaps greatly relaxed below the energy of direct laser excitation, with CO ($v = 1$–4). Since the C–O bond is not ruptured in the NO_2–CO reaction, deposition of energy into the vibrational mode should have little effect on the rate of reaction if the reaction is direct. However, if the reaction occurs via a long-lived complex, the energy in the C–O bond could be transferred to the appropriate bond of the complex, thereby inducing reaction. This situation occurs in the $O_3 + NO \rightarrow O_2 + NO_2$ (or NO_2^*) reaction, in which vibrational excitation of either O_3[33] or NO[34] seems to accelerate the reaction.

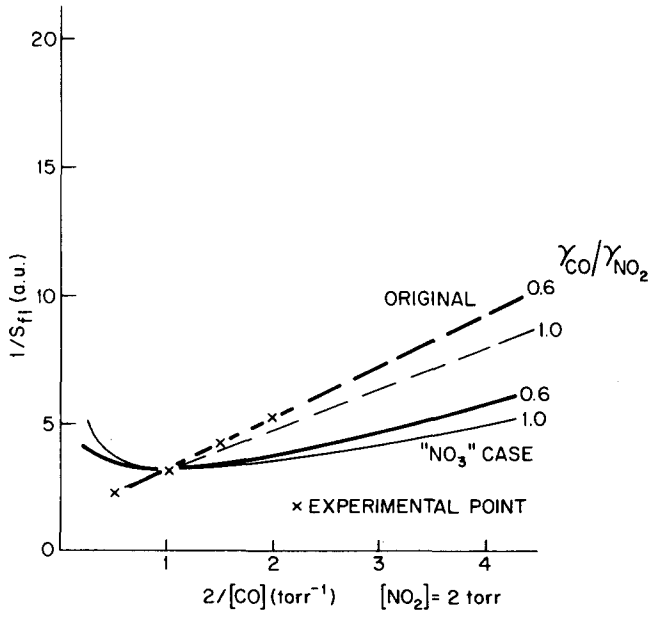

FIG. 7. Calculated $1/S_{f1}$ vs $1/[CO]$ ($[NO_2]$ fixed) behavior in "NO_3" and originally proposed mechanisms, alongside experimental data.

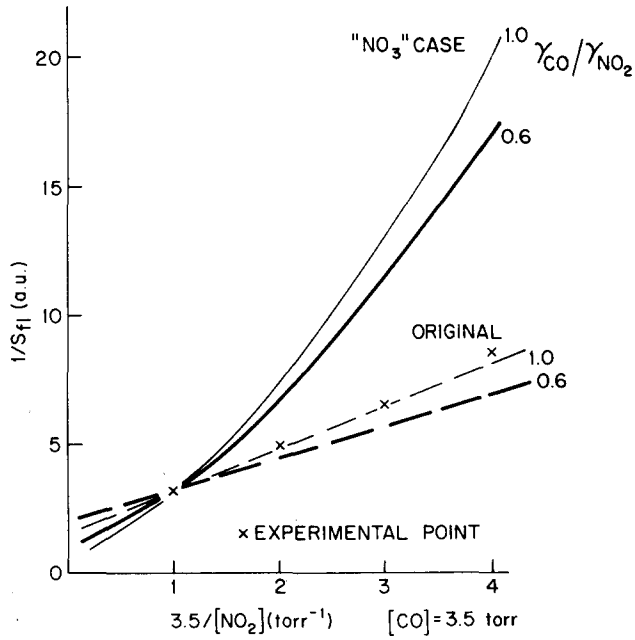

FIG. 8. Calculated $1/S_{f1}$ vs $1/[NO_2]$ ($[CO]$ fixed) behavior in "NO_3" and originally proposed mechanisms, alongside experimental data.

The kinetics of the proposed "$CO^\dagger$" mechanisms are outlined in Table III. A more detailed documentation and discussion of the nature of the various steps, along with relevant solutions of the kinetic equations, appears in Appendix B. Essentially, the overall process consists of five steps: NO_2 excitation, NO_2^* relaxation with subsequent CO ($v = 1$) excitation, very rapid $V-V$ equilibration in CO, slow decay of CO vibrational energy, and, lastly, reaction. Transfer of energy from NO_2^* to CO ($v = 0$), resulting in direct excitation of CO ($v > 1$), has been neglected; this assumption is consistent with the recent observation of Chu and Lin[35] that in collisions of CO ($v = 0$) with NO_2^*, excited with 5925 Å, the rate of transfer to CO ($v = 2$) is 0.006 times that to CO ($v = 1$). The calculation in Appendix B suggests that perhaps as many as 2×10^{-5} of all CO molecules are excited to $v \geq 5$. Since the results of Sec. V. E indicate that in this experiment only one in every 10^{11} collisions of *any* NO_2 with any CO molecule is reactive, there certainly appear to be enough suitably excited CO molecules to account for an NO_2–CO ($v \geq 5$) mechanism, even considering probable

TABLE III. Proposed $CO^\dagger$ mechanism.

	Rate constant
NO_2 excitation	
(1) $NO_2 + h\nu \rightarrow NO_2^*$	$\alpha I/\hbar\omega$
Relaxation and transfer	
(2) $NO_2^* \rightarrow NO_2 + h\nu$	γ_{rad}
(3) $NO_2^* + NO_2 \rightarrow NO_2 + NO_2$	γ_{NO_2}
(4) $NO_2^* + CO(v=0) \rightarrow NO_2 + CO(v=1)$	γ'_{CO}
(5) $NO_2^* + CO(v=0) \rightarrow NO_2 + CO(v=0)$	$\gamma_{CO} - \gamma'_{CO}$
$CO^\dagger$ equilibration	
(6) $CO(v=1) + CO(v=1) \rightarrow CO(v=0) + CO(v=2) + 27\ cm^{-1}$, etc.	Rapid CO V–V formation of $CO^\dagger$
$CO^\dagger$ relaxation	
(7) $CO^\dagger \rightarrow CO$	Slow decay (loss rate $= \Gamma[CO^\dagger]$)
Reaction	
(8) $NO_2 + CO(v \geq 5) \rightarrow NO + CO_2$	k_R'
(9) $NO_2^* + CO(v=1\text{–}4) \rightarrow NO + CO_2$	

steric factors; however, the calculated intensity dependence, which is proportional to the concentration of CO ($v \geq 5$) (Fig. 9), is as expected highly nonlinear, in disagreement with Fig. 3. Similar considerations rule out the influence of the NO_2^*–CO ($v=1$–4) reactions. For example, consider the case of NO_2^*–CO ($v=1$). Since CO ($v=1$) is directly pumped by NO_2^*, and since even after CO V–V equilibration most excitation remains in this level, both NO_2^* and CO ($v=1$) linearly depend on the laser intensity, therefore incorrectly predicting a quadratic reaction rate behavior with intensity. Though CO vibrational excitation does not appear to influence the production of CO_2 in this experiment, direct vibrational pumping of CO may still influence the NO_2–CO or NO_2^*–CO reactions.

VI. A MODEL OF THE LASER-STIMULATED REACTION

It is clear from the results of the previous section that the reaction of NO_2^* with CO is much slower than NO_2^* deactivation. Consequently, quantitative analysis of the reaction and, in particular, of the observed wavelength dependence requires a theory including both collisional relaxation and reaction dynamics. The observed reaction rate constant, now labeled as k_R^{obs}, may be formally expressed as

$$k_R^{obs}(\lambda) = \sum_{\substack{\text{states } i \\ E_i \geq E_{act}}}^{E_{max}=hc/\lambda} k_R(i) n(i) , \qquad (6)$$

where the sum is over energetically accessible states i between the activation and excitation energies, each with population $n(i)$ and reaction rate constant $k_R(i)$.

Analysis would be much less complicated if the reaction were performed at reactant concentrations low enough that NO_2^* would deactivate predominantly by either spontaneous emission or by collision with the wall. At such pressures only the directly laser-excited states of NO_2 would be available to react with CO. The radiative lifetime of NO_2 is, however, very long (75 μsec) and at the required pressures < 5 mtorr the rate of product formation would be extremely slow. Similar arguments make a molecular beam study of the NO_2^*–CO reaction fairly unattractive.

The exact pathway for deactivation of electronically excited NO_2 has not yet been determined. As described in Sec. V. E using laser-induced fluorescence Sakurai and Broida[17] were able to measure the net rate of collisional decay of the specific directly laser-excited $^2B_2$ states; however, to date no collision-induced lines have been observed in laser-induced fluorescence of NO_2.[36] Since collisions seem to induce only unresolvable quasi-continuum fluorescence, the present day description of $NO_2(^2B_2)$ relaxation is a statistical theory based on the behavior of this fluorescence.

Under low resolution Schwartz and Johnston[18] measured the pressure and wavelength dependence of both NO_2 visible fluorescence intensity and lifetime, using spectrometer filtered xenon arc lamp radiation (15 Å resolution) to excite pure NO_2. They observed that levels near the photon-excited states lost approximately two to three (average) vibrational quanta per collision. The apparent quenching rate was found to decrease as the difference of energy of the exciting and fluorescing photon increased. They successfully explained their data with the following model: All NO_2 vibrational modes are assumed to be strongly coupled; isoenergetic levels of $^2B_2$ and $\tilde{X}(^2A_1)$ are also strongly coupled by collision

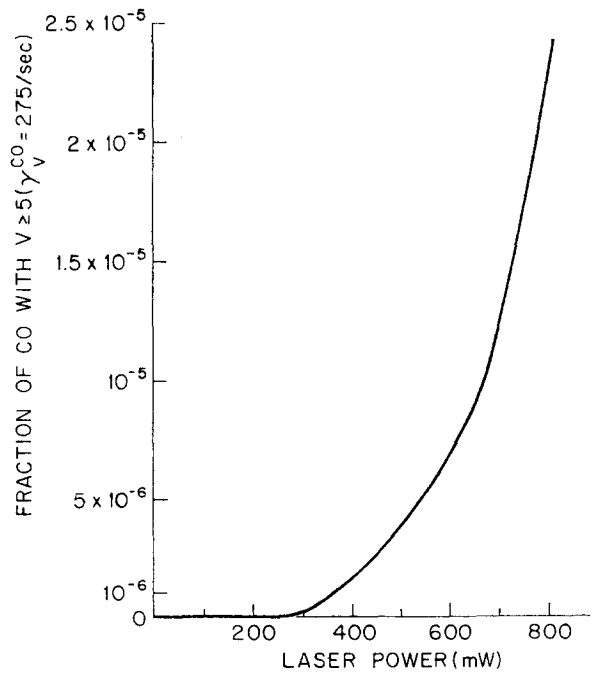

FIG. 9. Calculated fraction of reactive CO vs incident visible laser power in the "$CO^\dagger$" mechansim. Consult Appendix B for details. [In this Appendix this fraction of reactive CO is denoted as $f(I)$, which contains the laser intensity behavior expected in this mechanism for the experimental conditions of this study.]

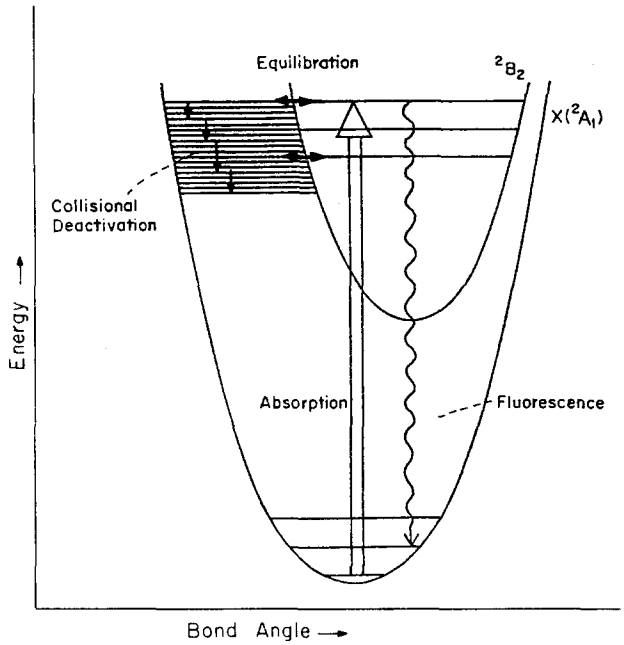

FIG. 10. Schematic diagram of deactivation pathways in NO_2^*.

and are populated according to their relative density of states; fluorescence occurs from only the $^2B_2$ state, but collisional relaxation occurs only down the vibrational ladder of $\tilde{X}(^2A_1)$, which is modeled as a triply degenerate vibrational mode. Direct electronic quenching of $^2B_2$ appears to be unimportant. In a very similar experiment Keyser *et al.*[37] fit the NO_2 fluorescence behavior using this same model, and similarly observed that on the average 1000 ± 500 cm^{-1} of vibrational energy was transferred from NO_2^* per collision.

Most of the assumptions in the Schwartz and Johnston model are physically reasonable. Since the $^2B_2$ state is apparently heavily perturbed by $\tilde{X}(^2A_1)$ states of the same vibronic symmetry, these two states should be strongly coupled by collision.[38] If these states are coupled, most vibrational relaxation should occur within the $\tilde{X}(^2A_1)$ manifold for several reasons. Since the two states are assumed to be populated according to their respective density of states, most of the population resides in the ground electronic state. In addition, the rate of relaxation within the $\tilde{X}(^2A_1)$ manifold is expected to be faster than in $^2B_2$ because of its larger vibrational quantum numbers and its more severe anharmonicity. Larger quantum numbers imply larger state-to-state relaxation cross sections because, in the harmonic oscillator approximation, this cross section is proportional to the quantum number of the higher state involved. Also, since in soft collisions vibrational quantum changes often follow the selection rules of radiative electric-dipole transitions, and since anharmonicity tends to relax these restrictions, relaxation is thereby allowed to more levels, causing an increase in the density of final states.

The weakest assumption in this model is the very important notion that within a given electronic state the three NO_2 vibrational modes are strongly coupled. The low-lying $\tilde{X}(^2A_1)$ levels involving the stretching modes ν_1 at 1320 cm^{-1} and ν_3 at 1617 cm^{-1} are probably well coupled with each other, but are most likely poorly coupled to the bending mode ν_2 at 750 cm^{-1} because of the lack of an energy resonance with either of these modes. However, the higher-lying $\tilde{X}(^2A_1)$ levels are probably well coupled to each other because of anharmonicity.

In the present analysis a statistical deactivation model similar to that of Schwartz and Johnston is employed. As is schematically depicted in Fig. 10, $^2B_2$ and $\tilde{X}(^2A_1)$ are equilibrated at every energy. Deactivation occurs within $\tilde{X}(^2A_1)$, fluorescence occurs from $^2B_2$, and, in an attempt to distinguish between $^2B_2$ and $\tilde{X}(^2A_1)$ reactivity, it is assumed that reaction with CO may occur with NO_2 in either of these two electronic states.

The three vibrational modes of $\tilde{X}(^2A_1)$ are approximated by a triply degenerate simple harmonic oscillator with a mode energy of $\epsilon = 0.15$ eV. This corresponds to 1210 cm^{-1}, which is nearly equal to both the average (1228 cm^{-1}) and geometric mean (1169 cm^{-1}) of the three actual modes. In the general case of t degenerate modes level i has degeneracy g_i given by

$$g_i = \frac{(i+t-1)!}{i!(t-1)!} \quad . \tag{7}$$

For NO_2 $t = 3$. The density of states predicted by this expression is in good agreement with the actual density for $i > 2$. The $^2B_2$ state is modeled in a similar manner. Though the exact mode energies are not known, the average spacing should be about the same as for $\tilde{X}(^2A_1)$. The ground state of $^2B_2$ is taken to be isoenergetic with level $i = m$ in $\tilde{X}(^2A_1)$, and therefore $[\tilde{X}(^2A_1), i]$ and $[^2B_2, i-m]$ are degenerate. Setting $m = 10$ fixes the $^2B_2$ energy at 1.5 eV, close to the value of 1.48 eV determined by Brand *et al.*[9] The results of the reaction model are fairly insensitive to the value of m.

The relative population of the degenerate $\tilde{X}(^2A_1)$ and $^2B_2$ levels, denoted as n_A and n_B, respectively, at energy $(i+3/2)\epsilon$ is determined by their relative density of states

$$n_B(i-m) = n_A(i)\,\frac{g_{i-m}}{g_i} \quad . \tag{8}$$

A steady-state, nonthermal balance exists near the laser-pumped level determined by the following rate equations:

$$\frac{dn_A(i)}{dt} = \gamma_{i+1\to i} n_A(i+1) - \gamma_{i\to i-1} n_A(i) = 0 \,,$$

with solution

$$n_A(i) = \frac{\gamma_{i+1\to i} n_A(i+1)}{\gamma_{i\to i-1}} = \frac{R}{\gamma_{i\to i-1}} \quad , \tag{9}$$

where R is the laser-pumping rate. $\gamma_{i+1\to i}$ is the rate of relaxation from $i+1 \to i$, which may be expressed as

$$\gamma_{i+1\to i} = \bar{\Gamma}(i+1) g_i \,, \tag{10}$$

where $\bar{\Gamma} = \gamma_{1\to 0}$. This is merely the product of the rate of transition between a pair of $i+1$ and i levels with the density of final states. As mentioned earlier the factor of $(i+1)$ is derived from the $i+1 \to i$ matrix element which, in the harmonic oscillator approximation, is $\sqrt{i+1}$ times the $1 \to 0$ matrix element. The density of

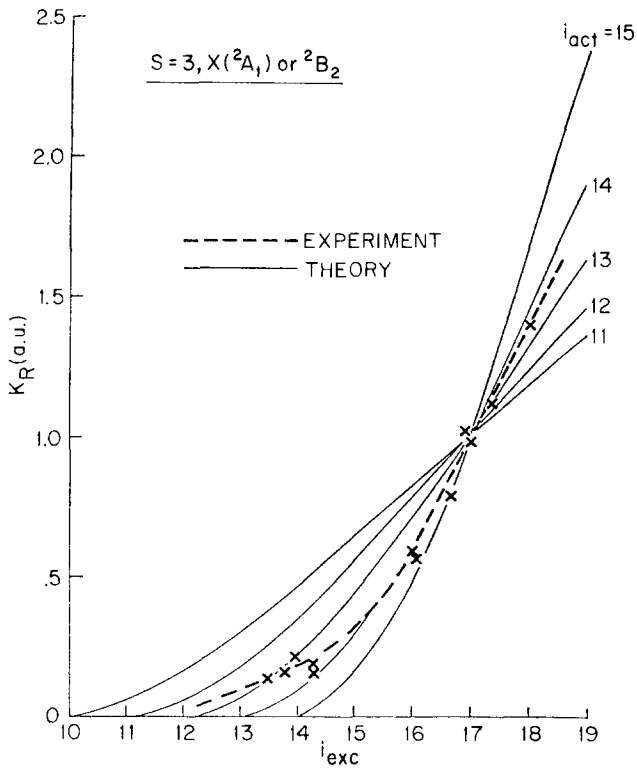

FIG. 11. Theoretical laser-initiated reaction rate vs level of excitation for $s = 3$ (direct reaction) and either the $\tilde{X}(^2A_1)$ or $^2B_2$ state responsible for reaction, alongside experimental results. For convenience the curves for different assumed values of the activation energy are normalized to 1 at $i = 17$, corresponding to 4880 Å. For precise correlation of the abscissa to true energy refer to the text and to Fig. 6.

states factor suggests that all "vibration collisional" selection rules between the original three modes have been relaxed. In addition, since R corresponds to the rate of laser pumping of NO_2, it is proportional to $[NO_2]$ for optically thin samples, while $\bar{\Gamma}$ is proportional to $\gamma_{CO}[CO] + \gamma_{NO_2}[NO_2]$.

Assigning a reaction rate constant of $k_A(i)$ to $[\tilde{X}(^2A_1), i]$ and $k_B(i-m)$ to $[^2B_2, i-m]$ and using Eqs. (7)–(10), Eq. (6) may be modified to predict the rate of CO_2 production:

$$\frac{d[CO_2]}{dt} = \frac{R[CO]}{\bar{\Gamma}} \sum_{i \geq i_{act}}^{i_{exc}} \frac{1}{(i+1)g_i} \left[k_A(i) + \frac{g_{i-m}}{g_i} k_B(i-m) \right] , \tag{11}$$

where i_{exc} and i_{act} refer to the levels associated with the exciting wavelength and the activation energy, respectively. As first mentioned in Sec. II. C it is clear that the pressure dependence of the reaction yield is independent of the details of the collisional relaxation and reaction scheme employed if $\gamma_{CO}/\gamma_{NO_2}$ is independent of i.

Since the potential curves for the NO_2–CO reaction have neither been measured nor calculated, a statistical theory, which requires less detailed energy curve information, rather than a dynamical theory, is employed to predict the reaction rate constants in Eq. (11). Specifically, RRK (Rice–Ramsperger–Kassel)[39] unimolecular decay theory is applied. This approach of employing these statistical models to both reactivity and relaxation is a refined version of the method adopted by Creel and Ross[22] in their study of the NO_2^*–NO_2 reaction. The above model is applied to two extreme cases. In one case the NO_2^*–CO reaction is considered to be a direct reaction, and the rate of reaction depends on the RRK distribution within the NO_2^*. In the other extreme RRK is applied to a $(NO_2CO)^*$ complex,[40] and the cross section for forming this complex is assumed to be both energy and state independent, while the reaction rate constant is proportional to the RRK unimolecular decay rate. The complex is implicitly assumed to have a definite lifetime, again independent of both energy and the nature of the state, after which time it decomposes to reform the reactants. The predictions of this statistical theory are used in an attempt to differentiate between $\tilde{X}(^2A_1)$ and $^2B_2$ reactivity by assuming that only one of the two states can promote reaction (in either of the two ways just discussed).

The activated complex or excited molecule with s vibrational degrees of freedom is treated as an s-fold degenerate oscillator. Judging from Herschbach *et al.*'s[30] estimate of the vibrational frequencies of a $(NO_2CO)^*$ complex the energy of level i may, to a reasonable approximation, be expressed as $E = (i + s/2)\epsilon$, where again $\epsilon = 0.15$ eV. Either one of the normal modes, or rather a specific linear combination of them, is responsible for reaction, and this degree of freedom is known as the reaction coordinate. When the energy in this mode, relative to zero-point fluctuations, is at least $E_{act} = i_{act}\epsilon$, reaction occurs at a rate proportional to the RRK unimolecular decay rate

$$k_R(i) = \bar{\omega} \frac{\dfrac{(i - i_{act} + s - 1)!}{(i - i_{act})!\,(s-1)!}}{\dfrac{(i+s-1)!}{i!\,(s-1)!}} , \tag{12}$$

where $\bar{\omega}$ is the geometric mean of the mode frequencies, and the second factor merely represents the fraction of energy rearrangements in which the reaction coordinate mode is suitably excited. This theory may be evaluated by employing Eq. (12) in the previous equation. If only the $\tilde{X}(^2A_1)$ state leads to reaction, $k_R(i)$ of Eq. (12) is proportional to $k_A(i)$ and k_B is set to zero. On the other hand, if only $^2B_2$ promotes reaction, Eq. (12) yields $k_B(i-m)$ with $i-m$ and $i_{act}-m$ substituted for i and i_{act}, respectively, and k_A set equal to zero. The variable s is not actually a free parameter. In a direct NO_2^*–CO reaction $s = 3$ (the number of NO_2 modes), whereas in the complex-forming reaction s equals the number of modes of the complex. $(NO_2CO)^*$ has nine degrees of vibration; however, as two of these are internal rotations, s should instead be set equal to seven.

The predictions of this model have been evaluated for various values of s and i_{act} and for either $\tilde{X}(^2A_1)$ or $^2B_2$ reacting. Some of these results are reproduced in Figs. 11–13, along with the experimental points. For the sake of clarity all curves have been normalized to 1.0 at $i = 17$, which closely corresponds to 4880 Å. Fair agreement is obtained for specific values of i_{act} for either $\tilde{X}(^2A_1)$ or $^2B_2$ reactivity for any value of s between 3 and

9; this model predicts identical results for $s = 3$ with either $\tilde{X}(^2A_1)$ or $^2B_2$ assumed to promote reaction. The data sharply disagrees with theory for s equal to either 1 or 2. Notice that for $i \gg i_{act}$ all theoretical curves are linear with energy in agreement with the experimental data obtained with argon-ion laser excitation.

Since this model is discrete in nature, an activation energy of $i_{act}\epsilon$ actually corresponds to a band of energies ranging from this value to $(i_{act} - 1)\epsilon$, and therefore the true activation energy associated with the value i_{act} is more nearly $(i_{act} - \frac{1}{2})\epsilon$. For $s = 3$, and either $\tilde{X}(^2A_1)$ or $^2B_2$ reactivity, E_{act} is 2.02 ± 0.08 eV. With $NO_2(^2B_2)$ as the reactive species the predicted activation energy decreases slowly with an increase in s, becoming about 1.87 eV for $s = 7$ and 9. With $\tilde{X}(^2A_1)$ the theoretically determined energy barrier decreases more rapidly with increasing s, falling to 1.72 eV at $s = 7$ and to about 1.57 eV at $s = 9$. Although the calculated curves best fit the data for the $s = 7$, $^2B_2$ case, the many assumptions inherent in the model and the balance between the influences on reactivity and relaxation of the two electronic states in this model [which destroys any change to truly differentiate between $\tilde{X}(^2A_1)$ and $^2B_2$ reactivity on a statistical basis] do not permit any decisive conclusions. The activation energy predicted by this model is somewhat higher than that of the thermal reaction, suggesting that these two reactions may proceed on different energy surfaces and that either there is a nonzero activation energy in $^2B_2$ or that either $^2B_1$ or $^2A_2$ is important.

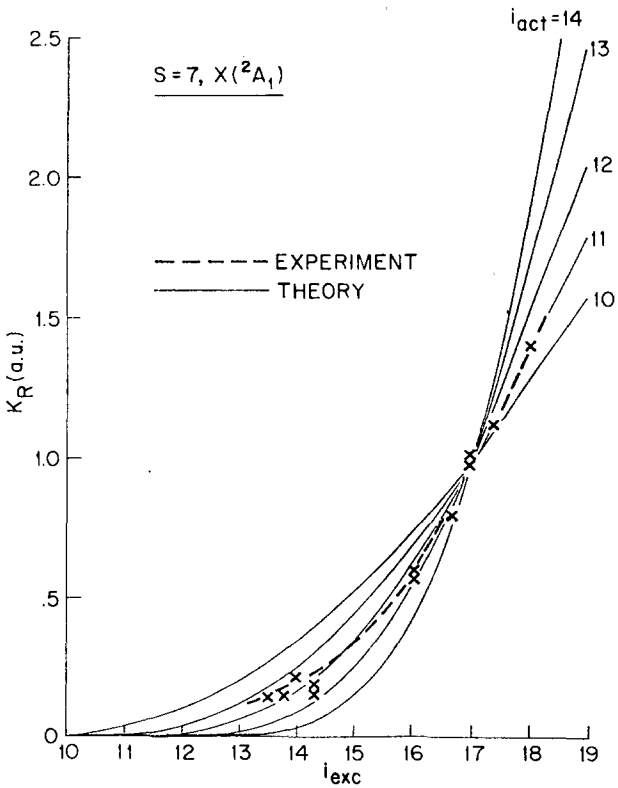

FIG. 12. Theoretical laser-initiated reaction rate vs level of excitation for $s = 7$ (complex reaction) and $\tilde{X}(^2A_1)$ reactivity (see Fig. 11 caption).

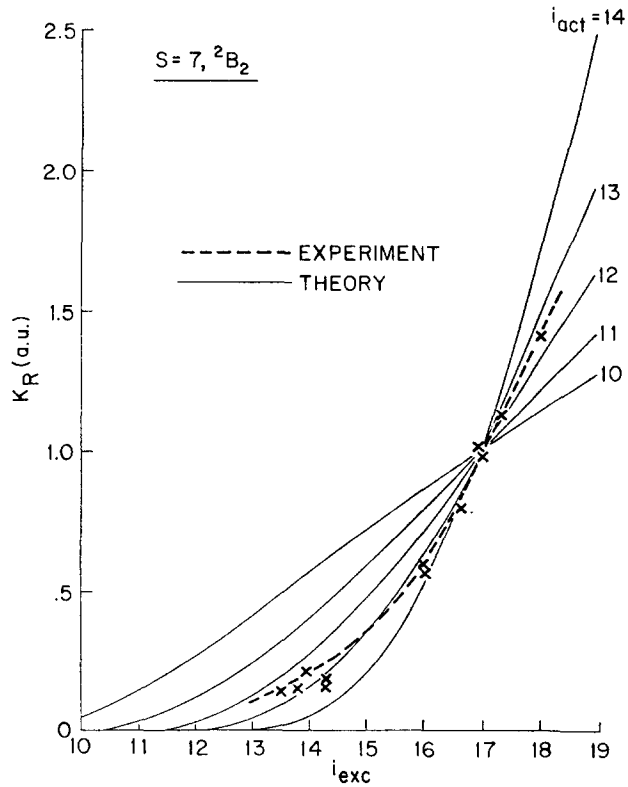

FIG. 13. Theoretical laser-initiated reaction rate vs level of excitation for $s = 7$ (complex reaction) and $^2B_2$ reactivity (see Fig. 11 caption).

VII. CONCLUSIONS

The kinetics observed in this study are in agreement with the mechanism proposed in Table I, in which NO_2^*–CO collisions create the products; RRK theory adequately describes this experimental behavior. Only one out of 80 000 collisions of laser-excited NO_2 with CO is reactive. Contributing factors to this small reaction cross section may be the dilution of the population of excited NO_2 into nonreactive states, the importance of CO internal excitation, or the translational energy barrier. These various possibilities might be tested by either a molecular beam study, direct vibrational heating of CO, or by thermal heating of the laser-excited reactants, respectively.

ACKNOWLEDGMENTS

One of the authors (I. P. H.) wishes to thank warmly the Fannie and John Hertz Foundation for financial support during his graduate studies at M.I.T. Thanks are also extended to C. L. Creel, R. W. Field, R. M. Osgood, Jr., and G. D. Gillispie for illuminating discussions and to L. W. Ryan, Jr. for invaluable technical assistance.

APPENDIX A

Of the several available techniques available for measuring the concentration of the CO_2 product LIF was chosen because of its ability to measure minute quantities of CO_2 and its insensitivity to small impurities of

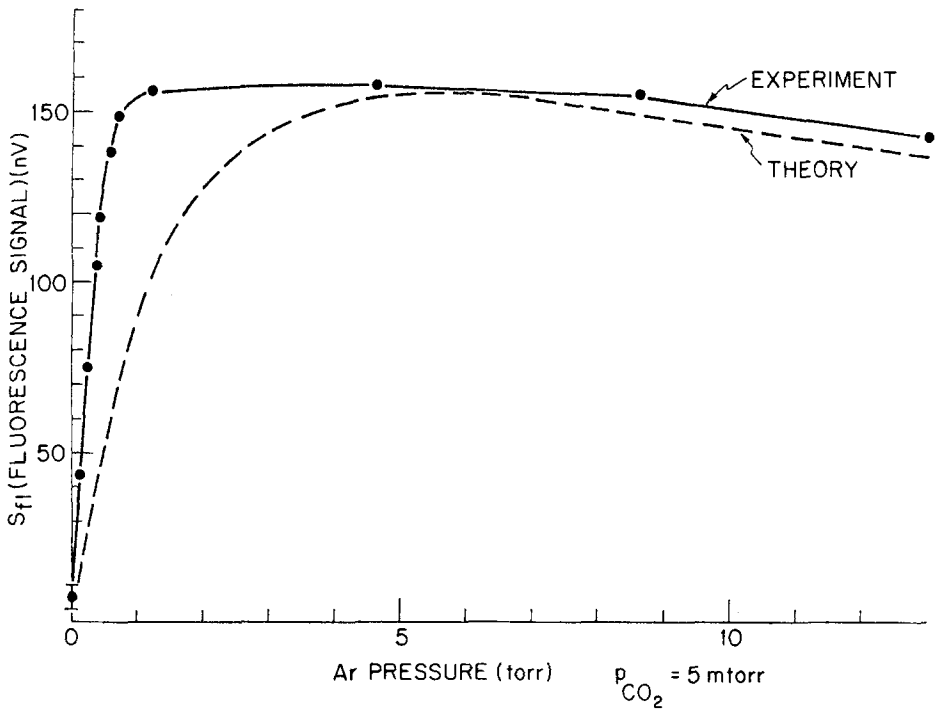

FIG. 14. The observed and calculated intensity of 4.3 μ CO_2 fluorescence S_{f1} as a function of argon buffer pressure, with p_{CO_2} =5 mtorr.

other molecules. Classical infrared absorption spectroscopy (at 4.3 μ) is not quite sensitive enough to measure the small amount of product. Direct measurement of the CO_2 pressure after distillation is susceptible to errors due to incomplete distillation of the reactants and of other products and due to the presence of unexpected products. Mass spectrometry and laser optoacoustic detection are both very sensitive and are competitive with LIF techniques; however, they require either relatively expensive or new technologies.

In this experiment the CO_2 concentration is measured only after the CO_2 has relaxed to its room temperature thermal distribution. Therefore, only one in 1000 CO_2 molecules are in the 10^00 vibrational level (see Fig. 1). Taking into account both the rotational partition function and a homogeneous linewidth one-tenth that of the Doppler width, at 1 mtorr only about 10^8 molecules/cc are in Doppler resonance with the laser. This, along with the known transition matrix elements, [41] predicts a very small absorption coefficient at 10.6 μ, of about 8×10^{-7}/(mtorr cm)$^{-1}$. Therefore, observation of the 4.3 μ fluorescence, amidst a very small thermal background, is much more sensitive than measuring the minute absorption at 10.6 μ. The relatively small reaction rate constant measured in this study, along with the large $NO_2^* + CO_2 \rightarrow NO_2 + CO_2^\dagger$ rate of vibrational excitation, [42] makes a measurement of the nascent CO_2 reaction product-vibrational level distribution unfeasible.

The kinetics of the fluorescence may be analyzed in two steps. First, the strong collisional coupling among the rotational levels of each vibrational level is considered, thereby reducing a many-level problem into a quasi-two-vibrational level system. Then, the processes describing relaxation of the relevant vibrational levels are considered. This problem may be decomposed in this manner because $R-T$ relaxation is much faster than $V-V$ and $V-TR$ collisional transfer, diffusional decay, and radiative decay. In addition, this grouping of the rapidly rotationally relaxed levels is experimentally relevant because the fluorescence from all (00^01), J states is being detected.

Feldman[43] has analyzed the coupling of two multilevel states in the rate equation approximation assuming that the rotational levels not directly involved in the laser transition are in thermal equilibrium. This analysis leads to a familiar result for the fluorescence intensity S_{f1}:

$$S_{f1} \propto \frac{\Delta\Omega}{4\pi}\left(\frac{e^{-(\Delta/\omega_D)^2}}{\sqrt{\pi}\,\omega_D}\right) n_{CO_2(10^00)} \sum_m \frac{\left(\frac{\mu_m E}{\hbar}\right)^2 \frac{\gamma_{rad}}{\gamma_1}}{\sqrt{1+\left(\frac{\mu_m E}{\hbar}\right)^2 \frac{1}{\gamma_2\gamma_R}}} \,. \tag{A1}$$

In this expression $\Delta\Omega$ is the subtended solid angle, Δ is the frequency detuning from linecenter, ω_D is the Doppler width, $n_{CO_2(10^00)}$ is the density of (10^00) levels [the thermal population of (00^01) is negligible], μ_m is the transition matrix element for the transition between the various m (i.e., J_g) components, E is the electric field amplitude, γ_{rad} is the rate of radiative decay, γ_1 is the total rate of decay of the (00^01) rotational level manifold, γ_2 is the polarization dephasing rate, and γ_R is the rotational relaxation rate. Excluding the saturation term in the denominator this expression is essentially the steady state population of (00^01), i.e., the rate of pumping (00^01) divided by the total rate of relaxation γ_1 multiplied by the spontaneous emission rate. Clearly, rotational relaxation affects only the saturation behavior. This expression is easily modified to include amplitude modulation of the CO_2 laser output, at radial frequency Ω, by substituting $\sqrt{\gamma_1^2+\Omega^2}$ for γ_1 in Eq. (A1).

The kinetics of this effective two-level system may

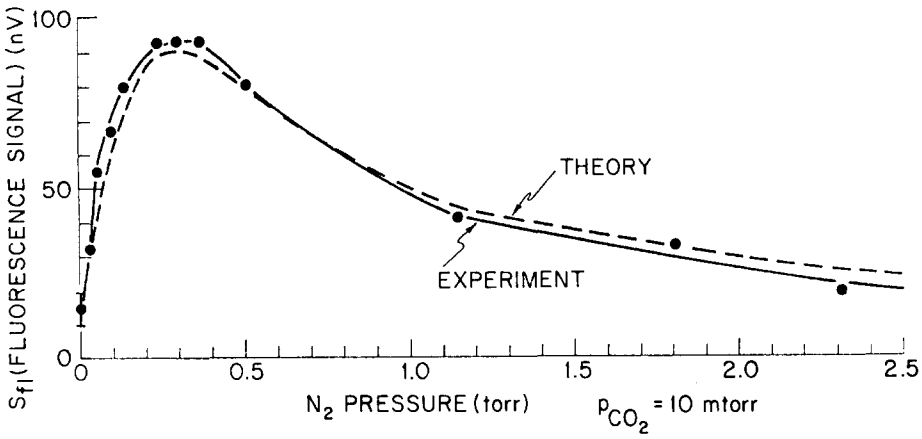

FIG. 15. The observed and calculated intensity of 4.3 μ CO_2 fluorescence S_{f1} as a function of nitrogen buffer pressure, with $p_{CO_2} = 10$ mtorr.

now be analyzed. Radiative decay γ_{rad}, collisional decay γ_V, and diffusional loss to the walls (or out of the detector's field of view) γ_{diff} all contribute to γ_1:

$$\gamma_1 = \gamma_{rad} + \gamma_V + \gamma_{diff} .$$

At the few mtorr CO_2 pressures of interest $\gamma_{rad} = 400$ sec^{-1}; radiative trapping is unimportant.[44] γ_V has contributions from the different collision partners X each at partial pressure p_X: $\gamma_V = \sum_X \Gamma_v^X p_X$. ($\Gamma_v^{CO_2} = 350$ $(sec\,torr)^{-1}$.[45-48]) Diffusion theory yields the result $\gamma_{diff} = \mu^2 D/r_0^2$,[49] where r_0 is the cell radius, D is the diffusion coefficient, where $D = D_0/p$ [D_0 for $CO_2(00^01)$ in $CO_2(00^00)$ is 0.066 cm^2/sec at 1 atm],[47,49] and $\mu^2 = 5.76$ if the mean free path is much smaller than r_0 (while it is smaller at lower pressures and in the free flow Knudsen regime).

In 1 mtorr pure CO_2 γ_1 is very large because of rapid transit to the walls, thus leading to a very small fluorescence signal. It was observed that the addition of a buffer gas at about 1 torr increases the detection sensitivity by well over an order of magnitude by significantly decreasing γ_1; the greatly reduced diffusion to the walls is accompanied by a minimal increase in collisional relaxation. Argon is an ideal buffer since it effectively confines $CO_2(00^01)$ ($D_0^{Ar} = 0.14$ cm^2/sec)[50] while vibrationally relaxing it only very slowly [$\Gamma_v^{Ar} = 48 \pm 4$ $(sec\,torr)^{-1}$][46,50] due to inefficient $V-T$ and intramolecular collisional relaxation. Nitrogen, on the other hand, enhances fluorescence much less than does argon because of near resonant $V-V$ transfer to $N(v=1)$ [$\Gamma_v^{N_2} = 16\,000$ $(sec\,torr)^{-1}$,[48] $D_0^{N_2} = 0.16$ cm^2/sec].

This behavior is experimentally verified in Figs. 14 and 15 in which S_{f1} vs p_{Ar}, with p_{CO_2} fixed at 5 mtorr, and S_{f1} vs p_{N_2}, with $p_{CO_2} = 10$ mtorr, are plotted (for the case of $\Omega = 691$ $(sec)^{-1}$, $P = 2$ W). These experimental traces are also compared to the above theory. γ_2 and γ_R were determined from the work of Meyers, Rhodes, and Haus[51] and $\langle \mu^2 \rangle_m$ was set equal to $\mu^2/2$, where $\mu = 2 \times 10^{-20}$ esu cm.[41] Actually, the above theory must be modified for the N_2 case to allow for the transfer of N_2 ($v=1$) excitation back to $CO_2(00^01)$. For $p_{CO_2} = 10$ mtorr and $p_{N_2} > 1$ torr this effect increases S_{f1} by 11%.

As discussed in Sec. IV this technique not only provides enhanced sensitivity but also linear calibration of S_{f1} vs p_{CO_2} and insensitivity to impurities. The calibration is linear because in Eq. (A1) γ_1, γ_2, and γ_R depend only on p_{Ar}, for $p_{Ar} \gg p_{CO_2}$, and γ_{rad} is a constant for $p_{CO_2} < 20$ mtorr, where radiative trapping is unimportant.

Experimentally, all $P(J)$ and $R(J)$ $J = 12-30$ (10.4 μ) lines led to approximately the same fluorescence intensity at equal laser power. However, during experimental runs care was exercised to insure single-line oscillation because laser saturation is important here and it is inherently nonlinear. The 9.4 μ lines led to larger signals than their 10.4 μ analogs, at equal power, because at room temperature (02^00) has 50% more population than (10^00).

The sensitivity of this LIF technique could be further increased by several orders of magnitude over the 0.1 mtorr sensitivity needed in this study by more judicious selection of a photodetector, by collecting a larger solid angle of fluorescence and by heating the CO_2 gas. Furthermore, it should be noted that fluorescence intensity could also be increased simply by transferring the CO_2 to a cell of very small volume, thereby increasing the CO_2 density. (In fact, in this experiment the detection cell was 4.5 times smaller than the reaction cell.)

APPENDIX B

The relevant processes in the proposed reaction mechanisms involving vibrationally excited CO were outlined in Sec. V. F and in Table III. Essentially, laser excited NO_2^* may transfer energy to CO ($v=1$) and then the CO vibrational ladder rapidly equilibrates via $V-V$ collisions. [The rate of Reaction (6) in Table III is $1.15 \pm 0.3 \times 10^5$ $(sec\,torr)^{-1}$.][52] Significant populations of CO ($v \geq 1$) may then be available to react with either NO_2 or NO_2^* because the CO vibrational manifold is only slowly relaxed. The study of Myers *et al.*[20] suggests that Reaction (4) in Table III is fairly efficient, with about half the energy transferred from NO_2^* to CO going into vibration, i.e., $\gamma'_{CO} \cong 0.5\,\gamma_{CO}$. Also, the experiments of Chu and Lin[35] confirm that direct excitation of CO ($v > 1$) is not very important in NO_2^*–CO ($v=0$) relaxation. Since the steady-state population of NO_2^* is much smaller than the calculated population of CO ($v=1$), the CO vibrational distribution is primarily determined by CO–CO collisions, and since $V-V$ transfer is very rapid, the resulting vibrational temperature T_v far exceeds the near-

ambient translational temperature T. Furthermore, since CO is anharmonic, the resulting vibrational distribution deviates from a Boltzmann, as is determined by[53]

$$n(v) = \frac{1}{Z} \exp\left(-\frac{vE_1}{k_B T_v}\right) \exp\left(-\frac{vE_1 - E_v}{k_B T}\right) , \quad \text{(B1)}$$

where Z is the vibrational partition function, and E_1 and E_v are the energies of the first and vth vibrational levels respectively.

There are several contributing factors to the relaxation of the $CO^\dagger$ manifold. The dominant loss of energy via radiative decay is due to $v=1 \rightarrow v=0$ at a rate of $33(\text{sec})^{-1}$,[54] while diffusional loss to the walls amounts to $140(\text{sec})^{-1}$ for a sample of 2 torr NO_2 and 4 torr CO under the conditions of this experiment. Both CO–CO and CO–NO_2, V–TR transfer have negligible rates[52]; CO ($v=1$)–NO_2 V–V transfer appears to be the dominant mode of $CO^\dagger$ relaxation. Though there is no experimental data available on this rate, analogy may be made to the cases of CO ($v=1$) transfer to SO_2 and CH_4, having measured relaxation rates of 25 and 3.3 μsec atm, respectively.[55] This suggests a NO_2–CO V–V rate of either $105(\text{sec})^{-1}$ (SO_2) or $880(\text{sec})^{-1}$ (CH_4) in a 2 torr NO_2–4 torr CO mixture, leading to a net $CO^\dagger$ decay rate Γ of either $275(\text{sec})^{-1}$ (SO_2) or $1050(\text{sec})^{-1}$ (CH_4). The CH_4 analogy is the more realistic of the two since the ν_3 mode of NO_2 (at 1617 cm^{-1}) and the ν_2 mode of CH_4 (at 1534 cm^{-1}) have about the same energy defect in exchange with the CO mode (2130 cm^{-1}), whereas SO_2 has a larger energy mismatch (ν_3 mode at 1362 cm^{-1}). In fact, if CO–NO_2 V–V transfer is much faster than overall V–TR, diffusion, and radiative losses, all three NO_2 modes and the CO mode may come into vibrational equilibrium, assuming that the NO_2 modes are strongly coupled. In harmonic oscillator approximation the vibrational temperature of any pair of modes T_a and T_b, having mode energies E_a and E_b, are then related by the well-known expression[53]

$$\frac{E_a}{T_a} - \frac{E_b}{T_b} = \frac{E_a - E_b}{T} , \quad \text{(B2)}$$

where T is again the translational temperature.

The specific case of ground state NO_2 reacting with CO excited to $v \geq 5$, i.e., above the NO_2–CO thermal barrier, may now be numerically examined. [This corresponds to Reaction (8) in Table III.] If all CO molecules with $v \geq 5$ (energy ≥ 1.3 eV) can promote reaction, the following rate law is obtained:

$$\frac{d[CO_2]}{dt} = k_R''[NO_2][CO]\left\{\frac{F(I)}{\Gamma} \frac{\gamma'_{CO}[NO_2]}{\gamma_{CO}[CO] + \gamma_{NO_2}[NO_2]}\right\} . \quad \text{(B3)}$$

In this relation the quantity in curly brackets is defined as $f(I)$, which represents the fraction of suitably vibrationally excited CO. $F(I)$ contains the explicit dependence of $f(I)$ on visible laser intensity. Since, as is discussed above, the main loss of CO vibrational energy appears to be due to V–V transfer to NO_2, Γ is proportional to $[NO_2]$, and this equation therefore predicts the same concentration dependence as the originally proposed mechanism in Eq. (1). The difference between the two mechanisms lies in the intensity behavior.

Both the expected intensity dependence and the actual number of suitably excited CO molecules, each closely related to $f(I)$, may be determined by first calculating the CO vibrational temperature T_v. Despite the small anharmonicity T_v may be obtained by equating the ensemble averaged harmonic oscillator energy to the average energy stored per molecule

$$\frac{E_1}{e^{E_1/k_B T_v} - 1} = \frac{I}{\hbar\omega}[NO_2] \frac{\gamma'_{CO}[CO]}{\gamma_{CO}[CO] + \gamma_{NO_2}[NO_2]} \frac{1}{\Gamma} \frac{1}{[CO]} . \quad \text{(B4)}$$

Each term on the right-hand side may be simply interpreted: The first term is the rate of pumping NO_2^*, the second partitions energy into CO ($v=1$), the third is the decay of CO vibrational energy, and the last term normalizes the total energy deposited into the average energy per molecular oscillator. Substituting the result of Eq. (B4) into (B1), $f(I)$ may be determined for 800 mW of 4880 Å, incident on the 2 torr NO_2–4 torr CO mixture under inspection, for the case of slow V–V transfer to NO_2 (SO_2 analogy) to be 2.3×10^{-5} and for the more rapid, and more likely, rate of transfer (CH_4 analogy) one obtains 3.6×10^{-8}. For the improbable case of complete V–V equilibration of NO_2–CO most of the depositied energy reappears in NO_2 because its mode energies are smaller than that of CO, leading to 1.9×10^{-15}. These results should be considered in light of $f(I=0)$ at room temperature (7.6×10^{-23}) which is essentially $n(v=5)$. The results described in Sec. V. E indicate that under the experimental conditions only one in every 10^{11} collisions of *any* NO_2 with *any* CO molecule is reactive. Assuming that the CO ($v \geq 5$)–NO_2 reaction has a steric factor of at least 100 this observation sets a lower limit of 10^{-9} on $f(I)$. There seems to be too few excited CO molecules in complete V–V equilibration to promote the reaction; however, if equilibration is incomplete, as is more likely, there appears to be sufficient $CO^\dagger$ molecules available for reaction; nonetheless, the intensity dependence predicted by the NO_2–CO ($v \geq 5$) mechanism, reproduced in Fig. 9 for the SO_2 V–V analogy, is as expected highly nonlinear, in disagreement with observations. As discussed in Sec. V. F the intensity behavior of proposed NO_2^*–CO ($v=1-4$) reactions also disagree with experiment.

[1]For example, consult the following reviews: J. T. Knudtson and E. M. Eyring, Ann. Rev. Phys. Chem. 25, 255 (1974); M. J. Berry, Ann. Rev. Phys. Chem. 26, 259 (1975); V. S. Letokov and C. B. Moore, Sov. J. Quantum Electron. 6, 129, 259 (1976).
[2]I. P. Herman, R. P. Mariella, Jr., and A. Javan, J. Chem. Phys. 65, 3792 (1976).
[3]G. M. Calhoun and R. H. Crist, J. Chem. Phys. 5, 301 (1937).
[4]F. B. Brown and R. H. Crist, J. Chem. Phys. 9, 840 (1941).
[5]H. S. Johnston, W. A. Bonner, and D. J. Wilson, J. Chem. Phys. 26, 1002 (1957).
[6]J. H. Thomas and G. R. Woodman, Trans. Faraday Soc. 63, 2728 (1967).
[7]Refer to Refs. 8–10 and to W. Demtröder, F. Paech, and R. Schmiedl, Chem. Phys. Lett. 26, 381 (1974); R. E. Smalley,

L. Wharton, and D. H. Levy, J. Chem. Phys. **63**, 4977 (1975); C. G. Stevens and R. N. Zare, J. Mol. Spectrosc. **56**, 167 (1975); T. Tanaka, R. W. Field, and D. O. Harris, J. Mol. Spectrosc. **56**, 188 (1975); J. C. D. Brand, W. H. Chen, and J. L. Hardwick, J. Mol. Spectrosc. **56**, 309 (1975); G. D. Gillispie and A. U. Khan, J. Chem. Phys. **65**, 1624 (1976).

[8]G. D. Gillispie, A. U. Khan, A. C. Wahl, R. P. Hosteny, and M. Krauss, J. Chem. Phys. **63**, 3425 (1975); refer also to C. F. Jackels and E. R. Davidson, J. Chem. Phys. **65**, 2941 (1976).

[9]J. C. D. Brand, J. L. Hardwick, R. J. Pirkle, and C. J. Seliskar, Can. J. Phys. **51**, 2184 (1973).

[10]J. L. Hardwick and J. C. D. Brand, Chem. Phys. Lett. **21**, 458 (1973).

[11]G. Herzberg, *Electronic Spectra of Polyatomic Molecules* (Van Nostrand Reinhold, New York, 1966).

[12]L. Burnelle, A. M. May, and R. A. Gangi, J. Chem. Phys. **49**, 561 (1968).

[13]G. D. Gillispie, Ph.D. Thesis, Michigan State University, 1975 (unpublished).

[14]It should be noted, however, that experimentally $O(^1D)$ is readily relaxed to $O(^3P)$ by $CO(X\,^1\Sigma^+)$. For example, see R. G. Shortridge and M. C. Lin, J. Chem. Phys. **64**, 4076 (1976). This indicates that a CO_2 complex is formed in which singlet and triplet CO_2 levels mix, thereby causing this nonadiabatic transition. This process is not important in this study since it relies on nearby triplet CO_2 levels, which are not accessible in this study since $O(^1D)$ is not actually formed.

[15]N. Cohen and J. Heicklen, J. Phys. Chem. **71**, 558 (1967).

[16]4545 Å predominantly excites a single $^2B_1$ level, J. L. Hardwick (private communication).

[17]K. Sakurai and H. P. Broida, J. Chem. Phys. **50**, 2404 (1969).

[18]S. E. Schwartz and H. S. Johnston, J. Chem. Phys. **51**, 1286 (1969).

[19]P. B. Sackett and J. T. Yardley, J. Chem. Phys. **57**, 152 (1972).

[20]G. H. Myers, D. M. Silver, and F. Kaufman, J. Chem. Phys. **44**, 718 (1966).

[21]Equation (2) may be derived by straightforward application of the heat conduction equation under the stated assumptions. This is discussed in more detail in I. P. Herman, Ph.D. Thesis, M.I.T., 1977 (unpublished).

[22]C. L. Creel and J. Ross, J. Chem. Phys. **64**, 3560 (1976).

[23]*Rate Constants of Gas Phase Reactions*, edited by V. N. Kondratiev (National Bureau of Standards, Washington, D. C., 1972).

[24]C. P. Fenimore, J. Am. Chem. Soc. **69**, 3143 (1947).

[25]T. C. Hall, Jr. and F. E. Blacet, J. Chem. Phys. **20**, 1745 (1952).

[26]A. Cabana, M. Laurin, W. J. Lafferty, and R. L. Sams, Can. J. Phys. **53**, 1902 (1975); R. L. Sams and W. J. Lafferty, J. Mol. Spectrosc. **56**, 399 (1975).

[27]The authors would like to thank Coherent Radiation for the loan of the dye laser.

[28]E. R. Murray, C. Kruger, and M. Mitchner, App. Phys. Lett. **24**, 180 (1974).

[29]The term bulk radiative lifetime is employed here since most of the fluorescence is emitted with this long lifetime. However, several fluorescence features have much shorter radiative lifetimes. For relevant discussions refer to Refs. 18 and 19, and to P. B. Sackett and J. T. Yardley, Chem. Phys. Lett. **9**, 612 (1971); R. Solarz and D. H. Levy, J. Chem. Phys. **60**, 842 (1974); F. Paech, R. Schmiedl, and W. Demtröder, J. Chem. Phys. **63**, 4369 (1975).

[30]D. R. Herschbach, H. S. Johnston, K. S. Pitzer, and R. E. Powell, J. Chem. Phys. **25**, 736 (1956).

[31]E. Leifer, J. Chem. Phys. **8**, 301 (1940).

[32]See, for example, *Fluorocarbons and the Environment—Report of the Federal Task Force on Inadvertent Modification of the Stratosphere, Council on Environmental Quality, Federal Council for Science and Technology, June* 1975 (U. S. GPO, Washington, D. C., 1975).

[33]R. J. Gordon and M. C. Lin, Chem. Phys. Lett. **22**, 262 (1973); R. J. Gordon and M. C. Lin, J. Chem. Phys. **64**, 1058 (1976); W. Braun, M. J. Kurylo, A. Kaldor, and R. P. Wayne, J. Chem. Phys. **61**, 461 (1974); M. J. Kurylo, W. Braun, C. N. Xuan, and A. Kaldor, J. Chem. Phys. **62**, 2065 (1975).

[34]J. S. Stephenson and S. M. Freund, J. Chem. Phys. **65**, 4303 (1976).

[35]D. Chu and M. C. Lin (to be published).

[36]K. Abé, J. Mol. Spectrosc. **48**, 395 (1973).

[37]L. F. Keyser, S. Z. Levine, and F. Kaufman, J. Chem. Phys. **54**, 355 (1971).

[38]W. M. Gelbart and K. F. Freed, Chem. Phys. Lett. **18**, 470 (1973). The authors point out that spectroscopically perturbed levels of mixed electronic state parentage are rapidly mixed by collisions. If such perturbations are very strong, the correlation diagrams for chemical reactions may lose some of their meaning and value. One of the purposes of this section is to examine the effect of these perturbations in the reaction under study, i.e., to see if it is possible to differentiate between the reactivity of the two supposedly perturbed states $^2B_2$ and $X(^2A_1)$.

[39]See, for example, H. S. Johnston, *Gas Phase Reaction Rate Theory* (Ronald, New York, 1966); E. E. Nikitin, *Theory of Elementary Atomic and Molecular Processes*, translated by M. J. Kearsley (Clarendon, Oxford, London, 1974); R. D. Levine and R. B. Bernstein, *Molecular Reaction Dynamics* (Clarendon, Oxford, New York, 1974).

[40]The possibility of an $(NO_2CO)^*$ forming in the NO_2–CO thermal reaction has been discussed in A. D. Walsh, Fuel **33**, 243 (1954).

[41]U. P. Oppenheim and A. D. Devir, J. Opt. Soc. Am. **58**, 585 (1968); H. P. Grieneisen, N. A. Kurnit, and A. Szöke, Opt. Commun. **3**, 259 (1971).

[42]The study of Meyers *et al.* (Ref. 20) suggests that molecules with relatively more vibrational degrees of freedom quench NO_2 visible fluorescence more efficiently than do molecules with fewer modes, implying that vibrational transfer is important. Since CO_2 was observed to relax NO_2 fluorescence as efficiently as NO_2, and more efficiently than diatomic molecules such as NO, NO_2^*–CO_2 quenching collisions probably vibrationally excite CO_2.

[43]B. J. Feldman, Ph.D. thesis, M.I.T., 1971 (unpublished).

[44]M. A. Kovacs and A. Javan, J. Chem. Phys. **50**, 4111 (1969).

[45]L. O. Hocker, M. A. Kovacs, C. K. Rhodes, G. W. Flynn, and A. Javan, Phys. Rev. Lett. **17**, 233 (1966).

[46]J. T. Yardley and C. B. Moore, J. Chem. Phys. **46**, 4491 (1967).

[47]M. Margottin-Maclou, L. Doyennette, and L. Henry, Appl. Opt. **10**, 1768 (1971).

[48]B. M. Cristophe and A. A. Offenberger, Can. J. Phys. **50**, 368 (1972).

[49]M. Kovacs, D. R. Rao, and A. Javan, J. Chem. Phys. **48**, 3339 (1968).

[50]M. A. Kovacs, Ph.D. thesis, M.I.T., 1969 (unpublished).

[51]T. W. Meyer, C. K. Rhodes, and H. A. Haus, Phys. Rev. A **12**, 1993 (1975).

[52]E. Weitz and G. Flynn, Ann. Rev. Phys. Chem. **25**, 275 (1974).

[53]C. E. Treanor, J. W. Rich, and R. G. Rehm, J. Chem. Phys. **48**, 1798 (1968).

[54]S. D. Rockwood, J. E. Brau, W. A. Proctor, and G. H. Canavan, IEEE J. Quantum Electron. **9**, 120 (1973). Though radiative decay from $v+1 \rightarrow v$ can be much faster, approaching 260 $(\text{sec})^{-1}$ for larger v, few molecules are in these states under the conditions of this experiment. The $1 \rightarrow 0$ rate is therefore most representative of radiative decay.

[55]M. A. Kovacs, J. Chem. Phys. **58**, 4704 (1973).